Femenias, G., Riera-Palou, F., Alvarez-Polegre, A. & Garcia-Armada, A. (2020). Short-Term Power Constrained Cell-Free Massive-MIMO Over Spatially Correlated Ricean Fading. *IEEE Transactions on Vehicular Technology*, 69(12), pp. 15200–15215.

DOI: 10.1109/tvt.2020.3037009

Short-Term Power Constrained Cell-Free Massive-MIMO over Spatially Correlated Ricean Fading

Guillem Femenias, *Senior Member, IEEE*, Felip Riera-Palou, *Senior Member, IEEE*, Alberto Álvarez-Polegre, *Student Member, IEEE*, and Ana García-Armada, *Senior Member, IEEE*

***Abstract*—This paper considers short-term power constrained cell-free massive multiple-input multiple-output (MIMO) scenarios where a large set of multi-antenna access points (APs) provide service to a group of single-antenna mobile stations (MSs) on a spatially correlated multipath environment. Based on a probabilistic approach, the spatially correlated propagation links are modeled using either Ricean or Rayleigh fading channel models that combine a *deterministic* line-of-sight (LOS) propagation path with a small-scale fading caused by non-line-of-sight (NLOS) multipath propagation. Assuming the use of minimum mean square error (MMSE) channel estimates, closed-form expressions for the downlink (DL) achievable spectral efficiency of a cell-free massive MIMO network with short-term power constraints (i.e., a *vector* normalized conjugate beamformer (NCB)) is derived and benchmarked against that provided by the conventional cell-free massive MIMO network with long-term power constraints (i.e., the conventional conjugate beamforming (CB)). These expressions, encompassing the effects of spatial antenna correlation, Ricean/Rayleigh fading and pilot contamination, are then used to devise both pragmatic and optimal max-min per-user power allocation strategies and to gain theoretical insight on the performance advantage provided by the use of short-term power constraints instead of the conventional long-term power constrained approach.**

I. Introduction

MASSIVE multiple-input multiple-output (MIMO) has emerged as one of the key physical layer pillars of the so-called 5G and beyond-5G cellular networks [1], [2]. Deploying tens, or even hundreds, of antennas at the base station (BS) to support multiple users on the same time-frequency resource, this technology has the potential to provide very high spectral and energy efficiencies by relying on rather simple signal processing and without the need for any BS cooperation [3]. Massive MIMO antenna arrays at the BSs have been traditionally arranged in compact collocated setups, but they can also be organized in spatially distributed configurations [1], [2], [4]. Distributed massive MIMO configurations are reminiscent of concepts such as distributed antenna system (DAS) [5], network MIMO [6], [7], coordinated multipoint (CoMP) transmission [8] or cloud radio access network (C-RAN) [9], but all of these arrangements can be essentially considered as different incarnations of a cooperative cellular infrastructure. Conceptually similar to the C-RAN and distributed massive MIMO architectures, but explicitly renouncing to the cellular network philosophy, an alternative distributed massive MIMO-based setup has been recently termed as *cell-free massive MIMO* [4], [10]. The underlying idea is that a massive number of access points (APs) distributed across the coverage area are connected to a central processing unit (CPU) and, as in the cellular collocated massive MIMO schemes, use very simple signal processing schemes to coherently serve a large number of mobile stations (MSs) on the same time-frequency resource. The distribution of APs over a large coverage area comes at the price of increased fronthaul capacity requirements but allows for an efficient exploitation of large-scale diversity and user proximity to offer a much higher coverage probability than collocated massive MIMO architectures [1], [2], [4], [10], [11].

The achievable spectral efficiency of cell-free massive MIMO systems has been rigorously characterized and optimized in papers such as, for instance, [4], [12]–[15]. Most of these research works, however, consider the use of single-antenna APs and the transmission over Rayleigh fading channels. Multi-antenna APs and communication over either spatially correlated Rayleigh fading channels or spatially uncorrelated Ricean fading channel models have also been dealt with in [16]–[21], just to name a few. As far as we know, however, none of these publications consider the analysis and optimization of the achievable spectral efficiency of a cell-free massive MIMO network using multi-antenna AP where the channels are characterized by spatially correlated Ricean fading. Moreover, when determining the power control coefficients to be used in the downlink (DL) segment, all previous research papers assume that the APs are constrained by a long-term average power requirement. It is well-known that power allocation strategies can be implemented assuming that power is constrained by either long-term or short-term average power constraints [22]. In the former strategy, averages are taken over both codewords and small-scale channel fading, whereas in the latter, averages are only taken over the codewords. According to regulatory bodies, such as the International Telecommunications Union (ITU) or the Federal Communications Commission (FCC), the transmit power in any time duration should not exceed a certain amount that depends on a large set of factors including, among many others, the application, the carrier frequency, the height of the antennas, or the population density.

G. Femenias and F. Riera Palou are with the Mobile Communications Group, University of the Balearic Islands (UIB), Ctra. de Valldemossa, km 7.5, Palma E-07122 (Illes Balears), Spain (email: guillem.femenias@uib.es, felip.riera@uib.es).

A. Álvarez Polegre and A. García Armada are with the Department of Signal Theory and Communications, Universidad Carlos III de Madrid, Avda. Universidad 30, 28911, Leganés (Madrid), Spain (email: aalvarez@tsc.uc3m.es, agarcia@tsc.uc3m.es).

Although these transmit power regulations can be captured by long-term power constraints, they are better suited, in practice, to short-term power constraints [22]. In [23], Interdonato *et al.* proposed a DL precoding scheme for cell-free massive MIMO scenarios with single-antenna APs, denoted as *normalized conjugate beamforming*, satisfying short-term power constraints at the APs, and they also derived an approximate closed-form expression for the DL achievable spectral efficiency. These researchers also showed that one of the main advantages of this precoding scheme over the conventional scheme based on long-term power constraints (i.e., conjugate beamforming) is the reduction of the beamforming gain uncertainty and, thus, the improvement of the well-known hardening ratio. This precoding scheme has been subsequently used in, for example, [24]–[26]. In [24], [25], however, Zhang *et al.* assume again the use of single-antenna APs, thus obviating the analytical complexity associated with multi-antenna spatially correlated Ricean fading channel models. In [26], Femenias *et al.* analyze the performance of a cell-free millimeter-wave (mmWave) massive MIMO network assuming the use of low-complexity hybrid digital-analog precoding filters where, aiming at simplifying the mmWave-based front-end, the analog precoding part implements a (constrained) statistical eigen beamformer that turns the multi-antenna APs into equivalent single-antenna equipment. The intrinsic analytical complexity of multi-antenna spatially correlated fading channels is thus, once more, avoided. This channel model has been previously considered by Özdogan *et al.* in the context of collocated massive MIMO scenarios [27], and by Álvarez-Polegre *et al.* in [28] in the context of cell-free massive MIMO with long-term power constraints.

Our main aim in this paper is to address some of the limitations shown by previous research work on this topic. In particular, the main contributions and novelty of this paper can be summarized as follows:

- As an important step forward with respect to previous research work on this topic, a novel closed form expression for the DL achievable spectral efficiency of a cell-free massive MIMO network based on normalized conjugate beamforming (NCB) (i.e., adhering to short-term average power constraints) is obtained in this paper. Notably, this expression is suitable for scenarios in which the APs are equipped with antenna arrays subject to spatially correlated fading channels. Previous works targeting this problem solely focused on the single-antenna case, a restriction that while greatly simplifying any performance analysis, precludes its application to the far more realistic multi-antenna AP considered here. Furthermore, depending on environmental factors, these channels are modeled as either Ricean or Rayleigh using a probabilistic approach. That is, compared to existing literature, a far more ellaborated analytical procedure is proposed that is able to cater for the realistic scenarios likely to be found in practical deployments (i.e., multi-antenna APs with spatial correlation, line-of-sight (LOS)/non-line-of-sight (NLOS) mixed propagation conditions).
- The closed-form expression for the DL achievable spectral efficiency, encompassing the effects of spatial antenna correlation, Ricean/Rayleigh fading and pilot contamination, is benchmarked against that provided by the conventional long-term power constrained cell-free massive MIMO network using conjugate beamforming (CB) and serves to gain theoretical insight on the performance advantage of using short-term power constraints in terms of achievable rate. The re-arrangement of the different terms in the rate expression further enables the derivation of closed-form metrics for the channel hardening effect and the favourable propagation condition (termed here, the channel hardening ratio and the favourable propagation ratio) that generalize previously known ones that were only applicable to simple propagation environments and ideal network assumptions (i.e., perfect channel state information (CSI), no pilot contamination). Moreover, by considering some special cases, valuable analytical insight is gained on how the different network parameters influence the both the channel hardening and favourable propagation metrics. Note that the channel hardening ratio metric is of capital importance to gain knowledge about how tight the achievable rates are to the true system performance and, in fact, the significant increase in hardening ratio NCB brings along implies that the optimization procedures governing the power and/or pilot allocation strategies can rely on tighter achievable rate closed-form expressions than in the CB counterpart. It is worth noting at this point that centralized beamforming techniques such as zero-forcing (ZF), regularized zero-forcing (RZF) or minimum mean square error (MMSE) have been shown to potentially outperform the CB-based distributed beamforming schemes [12], [18], [29]. Centralized beamformers, however, require that the APs invest a part of the capacity of the fronthaul links to transfer the CSI to the CPU and, moreover, that the CPU performs much more complex joint processing steps than those implemented at the APs when using a distributed beamforming strategy. Consequently, for conciseness, this paper focuses on distributed precoding architectures (NCB and CB) while leaving centralized precoders (ZF, RZF and MMSE) as a topic for further research.
- Using the mathematical expressions for the DL achievable rates, both pragmatic and optimal max-min per-user rate power allocation strategies are devised and their performance assessed. In particular, the closed-form expression for the DL achievable spectral efficiency, encompassing the effects of spatial antenna correlation, Ricean/Rayleigh fading and pilot contamination, is benchmarked against that provided by the conventional long-term power constrained cell-free massive MIMO network using CB and serves to gain theoretical insight on the performance advantage of using short-term power constraints in terms of achievable rate, channel hardening and favourable propagation under a large set of network configurations and propagation scenarios. In particular, results clearly show the performance advantage that Rice propagation brings along when compared to Rayleigh channels, while revealing the deleterious effects that spatial antenna correlation has on the network performance.

The rest of this paper is organized as follows. In Section II we describe the proposed system model, including the spatially correlated Ricean fading channel, the uplink (UL) channel estimation process, and the DL payload data transmission phase. Section III presents the theoretical analysis of the DL achievable rate for the NCB-based cell-free massive MIMO networks. Heuristic and max-min per-user rate power allocation strategies are proposed in Section IV. Heuristic power control is used to mathematically show that NCB hardens the effective channel gains at the MSs and, consequently, clearly outperforms the conventional CB strategy in terms of achievable spectral efficiency. Numerical results and discussions are provided in Section V and, finally, concluding remarks are summarized in Section VI.

Notation: Vectors and matrices are denoted by lower-case and upper-case boldface symbols. The q-dimensional identity matrix is represented by $\boldsymbol{I}_q$. The operator $\det(\boldsymbol{X})$ represents the determinant of matrix $\boldsymbol{X}$, whereas $\boldsymbol{X}^{-1}$, $\boldsymbol{X}^T$, $\boldsymbol{X}^*$ and $\boldsymbol{X}^H$ denote its inverse, transpose, conjugate and conjugate transpose (also known as Hermitian), respectively. The Euclidean norm of a vector $\boldsymbol{x}$ is denoted as $\|\boldsymbol{x}\|$. The expectation operator is denoted by $\mathbb{E}\{\cdot\}$. Finally, $\mathcal{CN}(\boldsymbol{m}, \boldsymbol{R})$ denotes a circularly symmetric complex Gaussian vector distribution with mean $\boldsymbol{m}$ and covariance $\boldsymbol{R}$, and $\mathcal{N}(0, \sigma^2)$ denotes a real valued zero-mean Gaussian random variable with standard deviation σ.

II. System model

Let us consider a cell-free massive MIMO system where M APs, each equipped with an array of N antennas, have been deployed over a large coverage area to simultaneously serve K single-antenna MSs on the same time-frequency resource. It is assumed that both APs and MSs are uniformly distributed over the coverage area and that all APs are connected to a CPU via error-free infinite-capacity fronthaul links. DL and UL transmissions are organized in a time division duplex (TDD) operation whereby each coherence interval[1] is split into an UL training phase, a DL payload data transmission phase and an UL payload data transmission phase. Note that assuming a perfect calibration of the hardware chains, the TDD operation guarantees UL/DL channel reciprocity. In the UL training phase, all MSs transmit UL training pilots allowing the APs to estimate the propagation channels to every MS in the network. Subsequently, these channel estimates are used to compute the precoding filters governing the DL payload data transmission and to detect the signals transmitted from the MSs in the UL payload data transmission phase. In this paper, sharing of CSI among APs will be avoided by using non-cooperative beamforming in the DL and matched filtering in the UL. Furthermore, and as it is commonly the case in most sub-6GHz setups, it will also be assumed that each antenna is connected to its own RF chain and, hence, that fully digital precoders/decoders can be implemented at the APs. For obvious reasons, the combined duration/bandwidth of the training, DL and UL phases, denoted as τ_p, τ_d and τ_u, respectively, should not exceed the coherence time/frequency of the channel, denoted as τ_c, that is, $\tau_p + \tau_d + \tau_u \leq \tau_c$, with all these parameters specified in samples (or channel uses) on a time-frequency grid. Note that, as we are interested in analyzing the effects a short-term power constraint at the APs may have on the performance of the cell-free massive MIMO architecture under spatially correlated fading channels, only the UL training phase and the DL payload data transmission phase will be explicitly considered in this paper.

[1]The coherence interval is a time-frequency window of duration and bandwidth equal to the coherence time and coherence bandwidth of the channel, respectively. This is the largest time-frequency window within which the channel response can be reasonably considered to be as invariant.

A. Channel model

As we consider spatially correlated Ricean fading, the vector $\boldsymbol{g}_{mk} \in \mathbb{C}^{N\times 1}$ characterizing the channel between the mth AP and MS k is modeled as

$$\boldsymbol{g}_{mk} = \overline{\boldsymbol{g}}_{mk} + \boldsymbol{R}_{mk}^{1/2}\boldsymbol{h}_{mk}, \tag{1}$$

where $\overline{\boldsymbol{g}}_{mk}$ is the LOS component, $\boldsymbol{h}_{mk} \sim \mathcal{CN}_N(\boldsymbol{0}, \boldsymbol{I}_N)$, and $\boldsymbol{R}_{mk}$ is a positive semi-definite covariance matrix that describes the spatial correlation of the NLOS components. As usual, the standard block fading model is assumed where $\boldsymbol{g}_{mk}$ is considered to be constant within a particular coherence interval and to vary independently between successive coherence intervals [30].

B. UL training phase: channel estimation

In each coherence interval, τ_p time/frequency samples (or channel uses) are reserved to perform UL pilot-based channel estimation at the APs. During this UL training phase, all K MSs simultaneously transmit pilot sequences of τ_p samples to the APs and thus, the $N \times \tau_p$ received UL signal matrix at the mth active AP is given by

$$\boldsymbol{Y}_{p_m} = \sqrt{\tau_p P_p}\sum_{k'=1}^{K}\boldsymbol{g}_{mk'}\boldsymbol{\varphi}_{k'}^T + \boldsymbol{N}_{p_m}, \tag{2}$$

where P_p is the transmit power of each pilot symbol, $\boldsymbol{\varphi}_k$ denotes the $\tau_p \times 1$ training sequence assigned to MS k, with $\|\boldsymbol{\varphi}_k\|^2 = 1$, and $\boldsymbol{N}_{p_m} \in \mathbb{C}^{N\times\tau_p}$ is a matrix of independent identically distributed (iid) zero-mean circularly symmetric Gaussian random variables with standard deviation σ_u. Ideally, training sequences should be chosen to be mutually orthogonal, however, since in most practical scenarios it holds that $K > \tau_p$, a given training sequence is assigned to more than one MS, thus resulting in the so-called pilot contamination, a widely studied phenomenon in the context of collocated massive MIMO systems [2], [31]. In this work it is assumed that training sequences are assigned to MSs using the following procedure:

- In scenarios where $K \leq \tau_p$, MSs are always assigned mutually orthogonal sequences.
- In scenarios where $K > \tau_p$, the fingerprinting training introduced in [26] is applied. This technique ensures that pilot sequences are reused only among users which are located far apart from each other, hence reducing the pilot contamination effects (see [26, Section V] for details).

Considering scenarios where MSs move slowly, it is reasonable to assume that the LOS components $\overline{\boldsymbol{g}}_{mk}$, and the scatter fading spatial correlation matrices $\boldsymbol{R}_{mk}$ can be accurately estimated and tracked in practice [17], [27], [30], [32]. In fact, the statistical distributions of the channel can be assumed to remain unchanged along with the active user population during multiple coherence intervals and, as suggested by Özdogan *et al.* in [27], they can be estimated in practice by using the sample mean and sample covariance matrices (see also [33], [34]). Furthermore, the same authors advocate that phase shifts of the LoS component resulting from small changes in the MS location will be identical for all BS antennas, and may therefore be accurately tracked[2]. Under these assumptions, we can define

$$\begin{aligned}\breve{\boldsymbol{y}}_{p\,mk} &= \left(\boldsymbol{Y}_{p_m} - \mathbb{E}\left\{\boldsymbol{Y}_{p_m}\right\}\right)\boldsymbol{\varphi}_k^* \\ &= \sqrt{\tau_p P_p}\sum_{k'=1}^{K}\boldsymbol{R}_{mk'}^{1/2}\boldsymbol{h}_{mk'}\boldsymbol{\varphi}_{k'}^T\boldsymbol{\varphi}_k^* + \boldsymbol{N}_{p_m}\boldsymbol{\varphi}_k^*\end{aligned} \tag{3}$$

and

$$\breve{\boldsymbol{g}}_{mk} = \boldsymbol{g}_{mk} - \mathbb{E}\left\{\boldsymbol{g}_{mk}\right\} = \boldsymbol{R}_{mk}^{1/2}\boldsymbol{h}_{mk}, \tag{4}$$

and then derive the MMSE estimate for the channel between the mth AP and the kth MS as [17], [35]

$$\begin{aligned}\hat{\boldsymbol{g}}_{mk} &= \overline{\boldsymbol{g}}_{mk} + \mathbb{E}\left\{\breve{\boldsymbol{y}}_{p\,mk}\breve{\boldsymbol{g}}_{mk}^H\right\}\left(\mathbb{E}\left\{\breve{\boldsymbol{y}}_{p\,mk}\breve{\boldsymbol{y}}_{p\,mk}^H\right\}\right)^{-1}\breve{\boldsymbol{y}}_{p\,mk} \\ &= \overline{\boldsymbol{g}}_{mk} + \sqrt{\tau_p P_p}\boldsymbol{R}_{mk}\boldsymbol{\Psi}_{mk}^{-1}\breve{\boldsymbol{y}}_{p\,mk},\end{aligned} \tag{5}$$

where

$$\boldsymbol{\Psi}_{mk} = \tau_p P_p\sum_{k'=1}^{K}\boldsymbol{R}_{mk'}\left|\boldsymbol{\varphi}_{k'}^H\boldsymbol{\varphi}_k\right|^2 + \sigma_u^2\boldsymbol{I}_N. \tag{6}$$

The channel estimate $\hat{\boldsymbol{g}}_{mk}$ and the MMSE channel estimation error $\tilde{\boldsymbol{g}}_{mk} = \boldsymbol{g}_{mk} - \hat{\boldsymbol{g}}_{mk}$ are uncorrelated random vectors distributed as $\hat{\boldsymbol{g}}_{mk} \sim \mathcal{CN}_N\left(\overline{\boldsymbol{g}}_{mk}, \boldsymbol{\Phi}_{mk}\right)$ and $\tilde{\boldsymbol{g}}_{mk} \sim \mathcal{CN}_N\left(\boldsymbol{0}, \boldsymbol{R}_{mk} - \boldsymbol{\Phi}_{mk}\right)$, respectively, where

$$\boldsymbol{\Phi}_{mk} = \tau_p P_p\boldsymbol{R}_{mk}\boldsymbol{\Psi}_{mk}^{-1}\boldsymbol{R}_{mk}^H. \tag{7}$$

C. DL payload data transmission phase

During the DL payload data transmission phase, the signal transmitted from AP m is given by

$$\boldsymbol{x}_m = \sqrt{P_d}\sum_{k=1}^{K}\eta_{mk}^{1/2}\boldsymbol{\varpi}_{mk}^T s_k, \tag{8}$$

where P_d is the transmit power available at the APs, $\boldsymbol{\varpi}_{mk} \in \mathbb{C}^{N\times 1}$ is the beamforming vector for MS k, s_k is the symbol transmitted to the kth MS, which satisfies $\mathbb{E}\left\{\left|s_k\right|^2\right\} = 1$, and η_{mk} is the DL (long-term) power allocation coefficient, chosen to meet the power constraint at the mth AP

$$\mathbb{E}\left\{\left\|\boldsymbol{x}_m\right\|^2\right\} \leq P_d, \tag{9}$$

[2]Note that all these assumptions, jointly with the block fading one, allow the analysis of the average (over time and frequency) performance of the network to be conducted by considering the one-shot probability distribution provided in (1).

where the expectation is taken over both the transmitted symbols (i.e., codewords) and the beamforming filters. For the specific case of the *classical* CB, the beamformer is defined as

$$\boldsymbol{\varpi}_{mk} = \hat{\boldsymbol{g}}_{mk}^*. \tag{10}$$

As this beamformer is not subject to a short-term normalization, averaging over it is tantamount to average over the estimated small-scale fading, P_d can only denote the *average* available transmit power, and (9) must represent an *average* (i.e., long-term) power constraint at the mth AP. The NCB for MS k, instead, is defined as

$$\boldsymbol{\varpi}_{mk} = \frac{\hat{\boldsymbol{g}}_{mk}^*}{\|\hat{\boldsymbol{g}}_{mk}\|}. \tag{11}$$

Owing to the normalization, after averaging over the transmitted symbols, the small-scale channel fading effects vanish. As a result, there is no need to average over the fast fading, thus allowing P_d to denote the available *instantaneous* transmit power, and (9) to represent a short-term power constraint at the mth AP. We note that, indeed, short-term transmit power constraints are most likely the ones to be required in practical deployments.

The received data signal at the kth MS can be expressed as

$$\begin{aligned}y_k &= \sum_{m=1}^{M}\boldsymbol{g}_{mk}^T\boldsymbol{x}_m + w_k \\ &= \sqrt{P_d}\sum_{m=1}^{M}\boldsymbol{g}_{mk}^T\sum_{k'=1}^{K}\eta_{mk'}^{1/2}\boldsymbol{\varpi}_{mk'}s_{k'} + w_k,\end{aligned} \tag{12}$$

where $w_k \sim \mathcal{CN}(0, \sigma_d^2)$ accounts for the receiver thermal noise. Assuming that only statistical CSI is available at the MSs, the received signal can be rewritten as [4]

$$y_k = \mathrm{DS}_k\, s_k + \mathrm{BU}_k\, s_k + \sum_{k'\neq k}^{K}\mathrm{UI}_{kk'}\, s_{k'} + w_k, \tag{13}$$

where

$$\mathrm{DS}_k = \sqrt{P_d}\sum_{m=1}^{M}\eta_{mk}^{1/2}\mathbb{E}\left\{\boldsymbol{g}_{mk}^T\boldsymbol{\varpi}_{mk}\right\}, \tag{14}$$

$$\mathrm{BU}_k = \sqrt{P_d}\sum_{m=1}^{M}\eta_{mk}^{1/2}\left(\boldsymbol{g}_{mk}^T\boldsymbol{\varpi}_{mk} - \mathbb{E}\left\{\boldsymbol{g}_{mk}^T\boldsymbol{\varpi}_{mk}\right\}\right), \tag{15}$$

and

$$\mathrm{UI}_{kk'} = \sqrt{P_d}\sum_{m=1}^{M}\eta_{mk'}^{1/2}\boldsymbol{g}_{mk}^T\boldsymbol{\varpi}_{mk'} \tag{16}$$

represent the strength of the desired signal, the beamforming gain uncertainty, and the strength of the interference term caused by the transmission to the k'th MS, respectively.

III. Achievable rates

DL achievable rates can be derived by using an analytical approach similar to those applied, for instance, in [2], [4], [23]. In particular, the sum of the second, third, and fourth terms in (13) is treated as *effective noise* (this is related to the well-known Gaussian assumption [36]). In fact, as the data symbols and thermal noise samples are zero-mean mutually

uncorrelated random variables (i.e., $\mathbb{E}\{s_k\} = \mathbb{E}\{w_k\} = 0$, for all k, and $\mathbb{E}\{s_k s_{k'}^*\} = \mathbb{E}\{s_{k'} w_k^*\} = 0$, for all k and k', it is straightforward to show that the additive terms constituting the *effective noise* are mutually uncorrelated (but not necessarily independent), and uncorrelated with the desired signal term. Consequently, recalling the fact that uncorrelated Gaussian noise represents the worst case, capacity bound described by Marzetta *et al.* in [2, Section 2.3.4] can be directly applied to obtain the DL achievable rate (measured in bits per second per Hertz) for MS k as

$$R_k^{\text{BF}} = \frac{\tau_d}{\tau_c} \log_2 \left(1 + \gamma_k^{\text{BF}}\right), \tag{17}$$

where $\text{BF} \in \{\text{NCB}, \text{CB}\}$ is a token used to represent either the normalized conjugate or the conjugate beamformer, and

$$\gamma_k^{\text{BF}} = \frac{|\text{DS}_k|^2}{\mathbb{E}\left\{|\text{BU}_k|^2\right\} + \sum\limits_{k' \neq k} \mathbb{E}\left\{|\text{UI}_{kk'}|^2\right\} + \sigma_d^2}. \tag{18}$$

In the following subsections we will elaborate on the mathematical analyzes related to the calculation of γ_k^{BF}. We will begin by introducing some useful results that will subsequently be used to obtain either approximate or exact closed-form expression for the DL achievable rates of short- and long-term power constrained cell-free massive-MIMO networks over spatially correlated Ricean fading.

A. Useful results

Lemma 1. *Given a circularly symmetric complex Gaussian vector $\boldsymbol{v} \sim \mathcal{CN}_N(\boldsymbol{0}, \boldsymbol{I}_N)$ and an arbitrary matrix $\boldsymbol{A} \in \mathbb{C}^{N \times N}$, the first and second (non-central) moments of the complex quadratic form $\mathcal{Q} = \boldsymbol{v}^H \boldsymbol{A} \boldsymbol{v}$ can be obtained as*

$$\mathbb{E}\{\mathcal{Q}\} = \text{tr}(\boldsymbol{A}) \tag{19}$$

and

$$\mathbb{E}\{|\mathcal{Q}|^2\} = |\text{tr}(\boldsymbol{A})|^2 + \text{tr}(\boldsymbol{A}\boldsymbol{A}^H), \tag{20}$$

respectively.

Lemma 2. *Given a complex Gaussian random vector $\boldsymbol{x} \sim \mathcal{CN}_N(\boldsymbol{\mu}, \boldsymbol{R})$ and an arbitrary matrix $\boldsymbol{M} \in \mathbb{C}^{N \times N}$, the first and second (non-central) moments of the complex quadratic form $\mathcal{Q} = \boldsymbol{x}^H \boldsymbol{M} \boldsymbol{x}$ can be obtained as*

$$\mathbb{E}\{\mathcal{Q}\} = \boldsymbol{\mu}^H \boldsymbol{M} \boldsymbol{\mu} + \text{tr}(\boldsymbol{R}\boldsymbol{M}) \tag{21}$$

and

$$\begin{aligned} \mathbb{E}\{|\mathcal{Q}|^2\} = &\left|\boldsymbol{\mu}^H \boldsymbol{M} \boldsymbol{\mu}\right|^2 + 2\Re\left\{\boldsymbol{\mu}^H \boldsymbol{M} \boldsymbol{R} \boldsymbol{M}^H \boldsymbol{\mu}\right\} \\ &+ 2\Re\left\{\boldsymbol{\mu}^H \boldsymbol{M} \boldsymbol{\mu}\, \text{tr}\left(\boldsymbol{R}\boldsymbol{M}^H\right)\right\} \\ &+ \left|\text{tr}\left(\boldsymbol{R}\boldsymbol{M}\right)\right|^2 + \text{tr}\left(\boldsymbol{R}\boldsymbol{M}\boldsymbol{R}\boldsymbol{M}^H\right), \end{aligned} \tag{22}$$

respectively.

Lemma 3. *Given a complex Gaussian random vector $\boldsymbol{x} \sim \mathcal{CN}_N(\boldsymbol{\mu}, \boldsymbol{R})$ and a Hermitian matrix $\boldsymbol{H} \in \mathbb{C}^{N \times N}$, the fractional (1/2)st (non-central) moment of the Hermitian quadratic form $\delta = \boldsymbol{x}^H \boldsymbol{H} \boldsymbol{x}$ can be accurately approximated as*

$$\mathbb{E}\{\delta^{1/2}\} \approx \frac{\sigma_\delta}{\sqrt{\mu_\delta}} \frac{\Gamma\left(\frac{\mu_\delta^2}{\sigma_\delta^2} + \frac{1}{2}\right)}{\Gamma\left(\frac{\mu_\delta^2}{\sigma_\delta^2}\right)}, \tag{23}$$

where, using Lemma 2,

$$\mu_\delta = \mathbb{E}\{\delta\} = \boldsymbol{\mu}^H \boldsymbol{H} \boldsymbol{\mu} + \text{tr}(\boldsymbol{R}\boldsymbol{H}) \tag{24}$$

and

$$\begin{aligned} \sigma_\delta^2 =& \mathbb{E}\left\{|\delta - \mathbb{E}\{\delta\}|^2\right\} = \mathbb{E}\{|\delta|^2\} - |\mathbb{E}\{\delta\}|^2 \\ =& 2\boldsymbol{\mu}^H \boldsymbol{H} \boldsymbol{R} \boldsymbol{H} \boldsymbol{\mu} + \text{tr}\left((\boldsymbol{R}\boldsymbol{H})^2\right). \end{aligned} \tag{25}$$

Proof. The proof is given in Appendix A. □

B. DL spectral efficiency of NCB

Let us define the Hermitian quadratic form $\delta_{mk} \triangleq \|\hat{\boldsymbol{g}}_{mk}\|^2$. As shown in Lemma 2 in Subsect. III-A, the first and second (non-central) moments of this quadratic form can be expressed as

$$\mu_{\delta_{mk}} = \mathbb{E}\{\delta_{mk}\} = \|\overline{\boldsymbol{g}}_{mk}\|^2 + \text{tr}\left(\boldsymbol{\Phi}_{mk}\right) \tag{26}$$

and

$$\sigma_{\delta_{mk}}^2 = \mathbb{E}\left\{|\delta_{mk} - \mu_{\delta_{mk}}|^2\right\} = 2\overline{\boldsymbol{g}}_{mk}^H \boldsymbol{\Phi}_{mk} \overline{\boldsymbol{g}}_{mk} + \text{tr}\left(\boldsymbol{\Phi}_{mk}^2\right). \tag{27}$$

These results can be used to state an approximate closed-form expression for the DL achievable rate of a cell-free massive MIMO network using short-term (i.e., NCB) power constraints over spatially correlated Ricean fading channels as:

Theorem 1 (Normalized Conjugate Beamforming)**.** *If NCB with $\boldsymbol{\varpi}_{mk} = \hat{\boldsymbol{g}}_{mk}^* / \delta_{mk}^{1/2}$ is used based on the MMSE channel estimation derived in* (5)*, then γ_k^{NCB} can be accurately approximated as in* (28)*, shown at the top of next page, with the token BF set to NCB, where $\rho_d = P_d/\sigma_d^2$,*

$$A_{mk}^{NCB} = \frac{\sigma_{\delta_{mk}}}{\sqrt{\mu_{\delta_{mk}}}} \frac{\Gamma\left(\frac{\mu_{\delta_{mk}}^2}{\sigma_{\delta_{mk}}^2} + \frac{1}{2}\right)}{\Gamma\left(\frac{\mu_{\delta_{mk}}^2}{\sigma_{\delta_{mk}}^2}\right)}, \tag{29}$$

$$\begin{aligned} B_{mk}^{NCB} =& \frac{\text{tr}\left(\left(\boldsymbol{R}_{mk} - \boldsymbol{\Phi}_{mk}\right)\left(\overline{\boldsymbol{g}}_{mk}\overline{\boldsymbol{g}}_{mk}^H + \boldsymbol{\Phi}_{mk}\right)\right)}{\mu_{\delta_{mk}}} \\ &+ \mu_{\delta_{mk}} - \left(A_{mk}^{NCB}\right)^2, \end{aligned} \tag{30}$$

$$\begin{aligned} C_{mkk'}^{NCB} =& \frac{1}{\mu_{\delta_{mk'}}} \Big[\overline{\boldsymbol{g}}_{mk}^H \boldsymbol{\Phi}_{mk'} \overline{\boldsymbol{g}}_{mk} + \text{tr}\left(\boldsymbol{R}_{mk}\boldsymbol{\Phi}_{mk'}\right) \\ &+ 2\Re\left\{\overline{\boldsymbol{g}}_{mk'}^H \overline{\boldsymbol{g}}_{mk}\, \text{tr}\left(\boldsymbol{R}_{mk}\boldsymbol{\Phi}_{mk'}\boldsymbol{R}_{mk'}^{-1}\right)\right\} \boldsymbol{\varphi}_k^H \boldsymbol{\varphi}_{k'} \\ &+ \left|\overline{\boldsymbol{g}}_{mk}^H \overline{\boldsymbol{g}}_{mk'}\right|^2 + \left|\text{tr}\left(\boldsymbol{R}_{mk}\boldsymbol{\Phi}_{mk'}\boldsymbol{R}_{mk'}^{-1}\right)\right|^2 \left|\boldsymbol{\varphi}_k^H \boldsymbol{\varphi}_{k'}\right|^2 \\ &+ \left|\overline{\boldsymbol{g}}_{mk}^H \boldsymbol{R}_{mk}^{1/2} \overline{\boldsymbol{g}}_{mk'}\right|^2 + \overline{\boldsymbol{g}}_{mk'}^H \boldsymbol{R}_{mk} \overline{\boldsymbol{g}}_{mk'}\Big] - \left|D_{mkk'}^{NCB}\right|^2, \end{aligned} \tag{31}$$

and

$$D_{mkk'}^{NCB} = \frac{\overline{\boldsymbol{g}}_{mk}^H \overline{\boldsymbol{g}}_{mk'} + \text{tr}\left(\boldsymbol{R}_{mk}\boldsymbol{\Phi}_{mk'}\boldsymbol{R}_{mk'}^{-1}\right) \boldsymbol{\varphi}_k^H \boldsymbol{\varphi}_{k'}}{A_{mk'}^{NCB}}. \tag{32}$$

Proof. The proof is given in Appendix B. □

$$\gamma_k^{\text{BF}} = \frac{\rho_d \left(\sum_{m=1}^{M} \eta_{mk}^{1/2} A_{mk}^{\text{BF}} \right)^2}{\rho_d \sum_{m=1}^{M} \eta_{mk} B_{mk}^{\text{BF}} + \rho_d \sum\limits_{\substack{k'=1 \\ k' \neq k}}^{K} \left(\sum_{m=1}^{M} \eta_{mk'} C_{mkk'}^{\text{BF}} + \left| \sum_{m=1}^{M} \eta_{mk'}^{1/2} D_{mkk'}^{\text{BF}} \right|^2 \right) + 1}, \tag{28}$$

C. DL spectral efficiency of the benchmarking precoder

Results in (26) and (27) can also be used to restate in the form of a theorem the exact closed-form expression for the DL achievable rate of a cell-free massive MIMO network using long-term (i.e., CB) power constraints over spatially correlated Ricean fading channels as [28]:

Theorem 2 (Conjugate Beamforming)**.** *If CB with $\boldsymbol{\varpi}_{mk} = \hat{\boldsymbol{g}}_{mk}^*$ is used based on the MMSE channel estimation derived in* (5)*, then γ_k^{CB} can be expressed as in* (28) *with the token BF set to CB, where*

$$A_{mk}^{CB} = \mathbb{E}\left\{\delta_{mk}\right\} = \mu_{\delta_{mk}}, \tag{33}$$

$$B_{mk}^{CB} = \sigma_{\delta_{mk}}^2 + \text{tr}\left(\left(\boldsymbol{R}_{mk} - \boldsymbol{\Phi}_{mk}\right)\boldsymbol{\Phi}_{mk}\right), \tag{34}$$

$$\begin{aligned} C_{mkk'}^{CB} =& \overline{\boldsymbol{g}}_{mk}^H \boldsymbol{\Phi}_{mk'} \overline{\boldsymbol{g}}_{mk} + \overline{\boldsymbol{g}}_{mk'}^H \boldsymbol{R}_{mk} \overline{\boldsymbol{g}}_{mk'} \\ &+ \left| \overline{\boldsymbol{g}}_{mk}^H \boldsymbol{R}_{mk}^{1/2} \overline{\boldsymbol{g}}_{mk'} \right|^2 + \text{tr}\left(\boldsymbol{R}_{mk} \boldsymbol{\Phi}_{mk'}\right), \end{aligned} \tag{35}$$

and

$$D_{mkk'}^{CB} = \overline{\boldsymbol{g}}_{mk}^H \overline{\boldsymbol{g}}_{mk'} + \text{tr}\left(\boldsymbol{R}_{mk} \boldsymbol{\Phi}_{mk'} \boldsymbol{R}_{mk'}^{-1}\right) \boldsymbol{\varphi}_k^H \boldsymbol{\varphi}_{k'}. \tag{36}$$

Proof. The proof can be readily obtained using [27] and [28] (see also derivations in the proof of Theorem 1). □

IV. Power control strategies

A. Heuristic power control scheme

In this set-up, as it was done by Interdonato *et al.* in [23], it is assumed that data signals are always transmitted with full average power (i.e., the power constraint in (9) is satisfied with equality). Furthermore, a fair comparison between NCB and CB is guaranteed by choosing the power control coefficients as

$$\eta_{mk} = \begin{cases} \frac{\mu_{\delta_{mk}}}{\sum_{k'=1}^{K} \mu_{\delta_{mk'}}}, & \text{NCB} \\ \frac{1}{\sum_{k'=1}^{K} \mu_{\delta_{mk'}}}, & \text{CB}, \end{cases} \tag{37}$$

for all $k \in \{1, \ldots, K\}$. Using the power control coefficients defined in (37), as was stated by Interdonato *et al.* in [23], ensures that the mth AP allocates the same amount of power to MS k under both NCB and CB strategies.

As a byproduct, the use of this pragmatic power control strategy can be very helpful in gaining some theoretical insight when comparing the performance of long-term and short-term power constrained precoding schemes under some particular scenarios. For instance, let us define the channel hardening ratio experienced by MS k as [37, Equation (10)]

$$\begin{aligned} \varrho_k^{\text{BF}} &= \text{Var}\left\{ \frac{\sum_{m=1}^{M} \eta_{mk}^{1/2} \boldsymbol{g}_{mk}^T \boldsymbol{\varpi}_{mk}}{\sum_{m=1}^{M} \eta_{mk}^{1/2} \mathbb{E}\left\{\boldsymbol{g}_{mk}^T \boldsymbol{\varpi}_{mk}\right\}} \right\} \\ &= \frac{\text{Var}\left\{\sum_{m=1}^{M} \eta_{mk}^{1/2} \boldsymbol{g}_{mk}^T \boldsymbol{\varpi}_{mk}\right\}}{\left(\sum_{m=1}^{M} \eta_{mk}^{1/2} \mathbb{E}\left\{\boldsymbol{g}_{mk}^T \boldsymbol{\varpi}_{mk}\right\}\right)^2} \\ &= \frac{\mathbb{E}\left\{\left|\text{BU}_k\right|^2\right\}}{\left|\text{DS}_k\right|^2} = \frac{\sum_{m=1}^{M} \eta_{mk} B_{mk}^{\text{BF}}}{\left(\sum_{m=1}^{M} \eta_{mk}^{1/2} A_{mk}^{\text{BF}}\right)^2}. \end{aligned} \tag{38}$$

Note that the term $\sum_{m=1}^{M} \eta_{mk}^{1/2} \boldsymbol{g}_{mk}^T \boldsymbol{\varpi}_{mk}$ represents the equivalent joint propagation channel (including the power control coefficient and the precoding filter) between the whole set of APs in the cell-free massive MIMO network and MS k. Hence, the lower the value of the channel hardening ratio, the higher the convergence of the instantaneous equivalent propagation channel to its mean (i.e., the higher the channel hardening experienced by MS k). Using (33) and (34), or (29) and (30), in (38), closed-form expressions for the channel hardening ratio of a generic MS k can be obtained for the CB, or NCB, schemes, respectively. Assuming the general spatially correlated Ricean fading channel model, however, it is very difficult to draw clear mathematical insight from the analysis of these expressions. Thus, let us explore the channel hardening ratio for both the NCB and CB schemes assuming a spatially uncorrelated Rayleigh fading channel model. In this particular case, $\overline{\boldsymbol{g}}_{mk} = \boldsymbol{0}$, $\boldsymbol{R}_{mk} = \beta_{mk} \boldsymbol{I}_N$, with β_{mk} denoting the large-scale propagation gain between the mth AP and MS k, and $\boldsymbol{\Phi}_{mk} = \gamma_{mk} \boldsymbol{I}_N$, where

$$\gamma_{mk} = \frac{\tau_p P_p \beta_{mk}^2}{\tau_p P_p \sum_{k'=1}^{K} \beta_{mk'} \left|\boldsymbol{\varphi}_{k'}^H \boldsymbol{\varphi}_k\right|^2 + \sigma_u^2}. \tag{39}$$

The channel hardening ratio for the CB scheme can then be expressed, using (37), as

$$\varrho_k^{\text{CB}} = \frac{\sum_{m=1}^{M} \frac{\beta_{mk} \gamma_{mk}}{\sum_{k'=1}^{K} \gamma_{mk'}}}{N \left(\sum_{m=1}^{M} \frac{\gamma_{mk}}{\sqrt{\sum_{k'=1}^{K} \gamma_{mk'}}} \right)^2}, \tag{40}$$

which is a decreasing function of N and M. In order to obtain a similarly manageable closed-form expression for the NCB scheme, let us assume that $\mu_{\delta_{mk}}^2 / \sigma_{\delta_{mk}}^2 \gg 1$. This is a fairly accurate assumption because we are assuming the use of a

high number of multiple-antenna APs. Under this assumption, as $\lim_{x\to\infty}\Gamma(x+\alpha)/\Gamma(x)=x^{\alpha}$, it holds that

$$A_{mk}^{\text{NCB}}=\frac{\sigma_{\delta_{mk}}}{\sqrt{\mu_{\delta_{mk}}}}\frac{\Gamma\left(\frac{\mu_{\delta_{mk}}^2}{\sigma_{\delta_{mk}}^2}+\frac{1}{2}\right)}{\Gamma\left(\frac{\mu_{\delta_{mk}}^2}{\sigma_{\delta_{mk}}^2}\right)}\approx\sqrt{\mu_{\delta_{mk}}} \tag{41}$$

and, consequently, the channel hardening ratio for the NCB scheme, assuming the pragmatic power control strategy proposed in (37), can be expressed as

$$\begin{aligned}\varrho_k^{\text{NCB}}&\approx\frac{\sum_{m=1}^{M}\frac{(\gamma_{mk}-\beta_{mk})\gamma_{mk}}{\sum_{k'=1}^{K}\gamma_{mk'}}}{N\left(\sum_{m=1}^{M}\frac{\gamma_{mk}}{\sqrt{\sum_{k'=1}^{K}\gamma_{mk'}}}\right)^2}\\&=\varrho_k^{\text{CB}}-\frac{\sum_{m=1}^{M}\frac{\gamma_{mk}^2}{\sum_{k'=1}^{K}\gamma_{mk'}}}{N\left(\sum_{m=1}^{M}\frac{\gamma_{mk}}{\sqrt{\sum_{k'=1}^{K}\gamma_{mk'}}}\right)^2}.\end{aligned} \tag{42}$$

That is, the channel hardening experienced by a generic MS k in a cell-free massive MIMO network using a short-term power constrained NCB is, for this particular pragmatic power control strategy, better than that experienced when using a long-term power constrained CB. Although this is only analytically shown for the Rayleigh case, Monte Carlo simulations presented in Section V show that this is also true for the Ricean scenario.

Tightly related to the *favourable propagation* concept described by Marzetta *et al.* in [2, Section 7.1], we define the favourable propagation ratio between MSs k and $k'\neq k$ as

$$\begin{aligned}\phi_{kk'}^{\text{BF}}&=\frac{\mathbb{E}\left\{\left|\text{UI}_{kk'}\right|^2\right\}}{\left|\text{DS}_k\right|^2}\\&=\frac{\sum_{m=1}^{M}\eta_{mk'}C_{mkk'}^{\text{BF}}+\left|\sum_{m=1}^{M}\eta_{mk'}^{1/2}D_{mkk'}^{\text{BF}}\right|^2}{\left(\sum_{m=1}^{M}\eta_{mk}^{1/2}A_{mk}^{\text{BF}}\right)^2}.\end{aligned} \tag{43}$$

The lower the value of the favourable propagation ratio, the lower the interference produced by the transmissions to MS k' on the signal received by MS k and hence, the more *orthogonal* can be considered to be the equivalent channels between the APs and MSs k and k'. As with the channel hardening ratio, using (33), (35) and (36), or (29), (31) and (32), in (43), closed-form expressions for the favourable propagation ratio between two generic MSs k and k' can be obtained for the CB, or NCB, schemes, respectively. Useful mathematical insight, however, can only be obtained by resorting to simplified scenarios such as the spatially uncorrelated Rayleigh fading channel model. In this particular case, it can easily be shown that both CB and NCB schemes provide identical exact (in the CB case) and approximate (in the NCB case) favourable propagation ratios, which can be expressed as

$$\begin{aligned}\phi_{kk'}^{\text{CB}}=\phi_{kk'}^{\text{NCB}}&=\frac{\sum_{m=1}^{M}\frac{\beta_{mk}\gamma_{mk'}}{\sum_{l=1}^{K}\gamma_{ml}}}{N\left(\sum_{m=1}^{M}\frac{\gamma_{mk}}{\sqrt{\sum_{l=1}^{K}\gamma_{ml}}}\right)^2}\\&+\left(\frac{\sum_{m=1}^{M}\frac{\gamma_{mk'}\beta_{mk}/\beta_{mk'}}{\sqrt{\sum_{l=1}^{K}\gamma_{ml}}}}{\sum_{m=1}^{M}\frac{\gamma_{mk}}{\sqrt{\sum_{l=1}^{K}\gamma_{ml}}}}\right)^2\left|\boldsymbol{\varphi}_k^H\boldsymbol{\varphi}_{k'}\right|^2.\end{aligned} \tag{44}$$

The first term of this ratio is a decreasing function of N and M. The second term, however, which is only different from zero when MSs k and k' share the same pilot sequence, does not depend on N and does not vanish with increasing M. Then, we can assert that both CB and NCB schemes provide favourable propagation among MSs that do not share the same pilot sequence. However, those MSs that share the same pilot training sequence will suffer from pilot contamination that ought to be combated by resorting to proper pilot and power allocation algorithms.

B. Max-min user rate power control

Max-min DL power allocation aims at finding the vector of power control coefficients $\boldsymbol{\eta}=[\boldsymbol{\eta}_1^T\ \dots\ \boldsymbol{\eta}_M^T]^T$, with $\boldsymbol{\eta}_m=[\eta_{m1}\ \dots\ \eta_{mK}]^T$ for all $m\in\{1,\dots,M\}$, that maximizes the minimum of the achievable rates (or, equivalently, the minimum of the achievable signal-to-interference-plus-noise ratios (SINRs)) of all MSs while satisfying the transmit power constraint at each AP [4], [10], [12]. This optimization problem can be generically formulated as

$$\begin{aligned}&\max_{\boldsymbol{\eta}\succeq\mathbf{0}}\ \min_k\gamma_k^{\text{BF}},\\&\text{subject to}\ \sum_{k'=1}^{K}\eta_{mk'}\mathbb{E}\left\{\left\|\boldsymbol{\varpi}_{mk'}\right\|^2\right\}\leq 1\quad\forall\, m,\end{aligned} \tag{45}$$

where

$$\mathbb{E}\left\{\left\|\boldsymbol{\varpi}_{mk'}\right\|^2\right\}=\begin{cases}1, & \text{NCB},\\ \mu_{\delta_{mk}}, & \text{CB}.\end{cases} \tag{46}$$

Using (18), problem (45) can be reformulated as

$$\begin{aligned}&\max_{\{\boldsymbol{\varsigma},\boldsymbol{\lambda}\}}\ \min_k\frac{\left(\sum_{m=1}^{M}\varsigma_{mk}A_{mk}^{\text{BF}}\right)^2}{\sum_{m=1}^{M}\sum_{k'=1}^{K}\varsigma_{mk'}^2\kappa_{mkk'}^{\text{BF}}+\sum_{\substack{k'=1\\k'\neq k}}^{K}\left|\lambda_{kk'}^{\text{BF}}\right|^2+\frac{1}{\rho_d}},\\&\text{subject to}\ \sum_{m=1}^{M}\varsigma_{mk'}D_{mkk'}^{\text{BF}}\leq\lambda_{kk'}\ \forall k'\neq k,\\&\qquad\sum_{k'=1}^{K}\varsigma_{mk'}^2\mathbb{E}\left\{\left\|\boldsymbol{\varpi}_{mk'}\right\|^2\right\}\leq 1\quad\forall\, m,\\&\qquad\varsigma_{mk}\geq 0\ \forall mk,\end{aligned} \tag{47}$$

where we have introduced the slack variables $\lambda_{kk'}$ and have used the definitions $\varsigma_{mk}=\eta_{mk}^{1/2}$ and

$$\kappa_{mkk'}^{\text{BF}}=\begin{cases}B_{mk}^{\text{BF}}, & k'=k\\ C_{mkk'}^{\text{BF}}, & k'\neq k.\end{cases} \tag{48}$$

TABLE I: Summary of default simulation parameters

Parameter	Value
Carrier frequency: f_0	2 GHz
Bandwidth: B	20 MHz
Side of the square coverage area: D	1000 m
Number of APs: M	100 APs
Noise figure (AP and MS): NF	9 dB
Available average power at the AP: P_d	200 mW
Available average power at the MS: P_p	100 mW
AP antenna height: h_{AP}	12.5 m
MS antenna height: h_{MS}	1.65 m
Coherence interval length: τ_c	200 samples
Training phase length: τ_p	20 samples
Payload phase length: $\tau_d = \tau_u$	$(\tau_c - \tau_p)/2$ samples
LOS reference distance: d_0	20 m
Pathloss parameters: α, β, σ_χ	
- Case LOS, $10m < d_{mk} \leq 150m$	34, 2.2, 3
- Case LOS, $d_{mk} > 150m$	-5.17, 4, 3
- Case NLOS	30, 3.67, 4
Shadow fading decorrelation distance: d_{dcorr}	9 m
Shadow fading correlation among APs:	0.5
Ricean K-factor distribution: μ_K, σ_K	9 dB, 5 dB
Distribution of the AoA deviation	$\zeta \sim \mathcal{N}(0, \sigma_\zeta^2)$
Angular standard deviation (ASD): σ_ζ	10°

As shown by Ngo *et al.* in [4, Appendix B], problem (47) is a quasi-concave optimization program that can be expressed in an equivalent form as

$$\begin{aligned} &\max_{\{\boldsymbol{\varsigma}, \boldsymbol{\lambda}^{\text{BF}}, x\}} \; x \\ &\text{s. t. } \sqrt{x} \left\| \left[\boldsymbol{\vartheta}_{1k}^{\text{BF}} \dots \boldsymbol{\vartheta}_{Mk}^{\text{BF}} \; \overline{\boldsymbol{\lambda}}_k^{\text{BF}} \; \frac{1}{\sqrt{\rho_d}} \right] \right\| \leq \sum_{m=1}^{M} \varsigma_{mk} A_{mk}^{\text{CB}} \; \forall k, \\ &\quad \sum_{m=1}^{M} \varsigma_{mk'} D_{mkk'}^{\text{BF}} \leq \lambda_{kk'}^{\text{BF}} \; \forall k' \neq k, \\ &\quad \sum_{k'=1}^{K} \varsigma_{mk'}^2 \mathbb{E}\left\{ \left\| \boldsymbol{\varpi}_{mk'} \right\|^2 \right\} \leq 1 \quad \forall m, \\ &\quad \varsigma_{mk} \geq 0 \; \forall mk, \end{aligned} \tag{49}$$

where $\boldsymbol{\vartheta}_{mk}^{\text{BF}} = \left[\varsigma_{m1} \sqrt{\kappa_{mk1}^{\text{BF}}} \dots \varsigma_{mK} \sqrt{\kappa_{mkK}^{\text{BF}}} \right]$ and $\overline{\boldsymbol{\lambda}}_k^{\text{BF}} = \left[\lambda_{k1}^{\text{BF}} \dots \lambda_{k(k-1)}^{\text{BF}} \lambda_{k(k+1)}^{\text{BF}} \dots \lambda_{kK}^{\text{BF}} \right]$. Problem (49) is a second order cone (SOC) program that can be efficiently solved by using a conventional iterative bisection search algorithm. Specific details on the optimality, complexity and feasibility of these algorithms were fully commented by Ngo *et al.* in the seminal paper [4]. In particular, it is worth pointing out that the optimization of the power coefficients depends only on large-scale fading parameters, whose rate of variation is on the order of many coherence times (at least 40-50 according to [4]). Consequently, given its low rate of execution, the complexity of this optimization procedure becomes relatively unimportant.

V. Numerical Results

Similar to the simulation scenario setups typically used in most of the relevant literature on cell-free massive MIMO networking (see, for instance, [4], [10], [12], [14]–[16], [18], [23]), APs and MSs are uniformly distributed at random within a square coverage area of size $D \times D$ m^2. Furthermore, in order to simulate the effects of operating an infinite coverage area network, this square area is wrapped-around at the edges.

The link between the mth AP and the kth MS will be considered to be either in LOS or NLOS, with the LOS probability being given by [38]

$$p_{\text{LOS}}(d_{mk}) = \min\left(1, \frac{d_0}{d_{mk}} + \left(1 - \frac{d_0}{d_{mk}}\right) e^{-\frac{d_{mk}}{2d_0}}\right), \tag{50}$$

where d_0 is a reference distance and d_{mk} is the distance between AP m and MS k. The propagation losses (measured in dB) characterizing the propagation link between the mth AP and the kth MS will be modelled as

$$L_{mk} = \alpha + 10\beta \log_{10}(d_{mk}) + \chi_{mk}, \tag{51}$$

where $\chi_{mk} \sim \mathcal{N}\left(0, \sigma_\chi^2\right)$ is the shadow fading component, and the values of parameters α, β and σ_χ depend on whether the corresponding link is in LOS or NLOS. The spatial correlation model for the shadow fading experienced by the different propagation links is described in [4, (54)-(55)].

Each AP will be assumed to be equipped with a uniform linear array (ULA) with half-wavelength antenna spacing. Hence, defining $\beta_{mk} = 10^{-L_{mk}/10}$, the LOS component of the propagation channel between MS k and AP m can be expressed as

$$\overline{\boldsymbol{g}}_{mk} = \sqrt{\frac{K_{mk}}{K_{mk}+1}\beta_{mk}} \left[1 \; e^{j\zeta_{mk}} \dots e^{j(N-1)\zeta_{mk}}\right]^T, \tag{52}$$

where K_{mk} is the Ricean K-factor, with $K_{mk} = 0$ for NLOS propagation links and $10\log_{10}(K_{mk}) \sim \mathcal{N}\left(\mu_K, \sigma_K^2\right)$ for LOS propagation links, and $\zeta_{mk} = \pi \sin\psi_{mk}$, with ψ_{mk} denoting the angle of arrival (AoA) of the signal transmitted by MS k seen from the mth AP. The covariance matrix characterizing the NLOS small-scale fading will be obtained by using the well-known local scattering spatial correlation model [30, 2, Sec. 2.6]. In particular, the (p,q)th component of the Toeplitz matrix $\boldsymbol{R}_{mk}$ will be computed as [30, 2, eq. (2.23)]

$$[\boldsymbol{R}_{mk}]_{p,q} = \frac{\beta_{mk}}{K_{mk}+1} \int_{-\infty}^{+\infty} e^{j\pi(p-q)\sin(\psi_{mk}+\zeta)} f_\zeta(\zeta) d\zeta, \tag{53}$$

where $f_\zeta(\zeta)$ is the probability density function (pdf) of the angular deviation of the different propagation paths of the local scatterer around the MS with respect to the nominal AoA. Typical distributions for the angular deviation that can be found in the literature (see [30, 2, Sec. 2.6] and references therein) are the Gaussian distributed deviations $\zeta \sim \mathcal{N}(0, \sigma_\zeta^2)$, the Laplace distributed deviations $\zeta \sim \text{Lap}\left(0, \sigma_\zeta/2\right)$ or the uniformly distributed deviations $\zeta \sim \mathcal{U}\left[-\sqrt{3}\sigma_\zeta, \sqrt{3}\sigma_\zeta\right]$, with σ_ζ representing the angular standard deviation (ASD) around the nominal AoA. In spite of its simplicity, this channel model captures the key characteristics of spatial correlation in massive MIMO scenarios and provides qualitative results that are fully consistent with those obtained using other state-of-the-art channel models [30], [39].

Default parameters used to set-up the simulation scenarios under evaluation are summarized in Table I and are inspired by prior research works on this topic (see, for instance, [4], [18], [38] and references therein). Moreover, except otherwise

stated, the dissimilarity cluster-based pilot assignment (DCPA) scheme described in [26] is used to allocate the available training sequences to MSs. In words, the CPU has perfect knowledge of vector $\boldsymbol{\beta}_k = [\beta_{1k} \ \ldots \ \beta_{Mk}]$ for any MS k in the network. This vector, containing the large-scale propagation gains of the channels linking MS k to the M APs, can be regarded as a *fingerprint* characterizing MS k. The DCPA scheme uses the cosine similarity measure to ensure that pilot sequences are only reused, in a balanced manner, by MSs showing the most dissimilar large-scale propagation patterns to the APs.

Figure 1 shows the cumulative distribution function (CDF) of the achievable per-user rate obtained using NCB and CB for the specific case of $K = 25$ MSs and $M = 100$ APs when using either pragmatic (see Fig. 1a) or max-min (see Fig. 1b) power allocation under two different channel environments, the correlated Rayleigh fading model (previously reported in the literature and shown here in dashed lines) and the more realistic spatially correlated channel subject to Ricean fading (solid lines). The upper subplots correspond to a configuration where APs are equipped with $N = 2$ antennas whereas the lower subplots represent the case when $N = 8$ antennas are available at each AP. Most notably, and irrespective of any other parameter, large differences are observed between the Rayleigh and Ricean fading scenarios, thus revealing the importance of considering the use of spatially-correlated Ricean fading channel models when analyzing ultradense networks such as those postulated by the cell-free massive MIMO paradigm. Assuming the use of the pragmatic power allocation strategy, per-user achievable rate performance when APs are equipped with few antennas ($N = 2$, upper subplot in Fig. 1a) always favours the existence of the LOS component thus making the Ricean environment preferable over the Rayleigh one. In contrast, when APs are equipped with a large number of antennas (e.g., $N = 8$, lower subplot in Fig. 1a), worst users (lowest 15%-ile and 35%-ile ranges, for CB and NCBs, respectively) benefit from NLOS propagation as the large number of antennas per AP already provides a considerable degree of channel hardening with lower correlation (i.e., more diversity) than the Ricean propagation counterpart. It is worth noting, also, that the NCB, using short-term power constraints, clearly outperforms the CB, using long-term power constraints, regardless of the channel model or the number of antennas at the APs. The superiority of the NCB precoder is further reinforced by results presented in Fig. 1b where the use of max-min power allocation is assessed. As it always occurs with max-min power allocation, the per-user rate CDF curves present a much steeper shape than those obtained using other power allocation strategies owing to the fact that, for each channel realization, all MSs in the network attain a common rate. Furthermore, note how NCB offers a very significant advantage over CB irrespective of the number of antennas and propagation conditions. In particular, and unlike the pragmatic power allocation case, max-min performance in spatially correlated Ricean fading is always beneficial irrespective of the rate-percentile under evaluation.

The average per-user rate of NCB and CB is now assessed in Fig. 2a as a function of the number of MSs in a cell-free massive MIMO network with $M = 100$ APs all equipped with $N = 4$ antennas. Results obtained under spatially correlated Rayleigh (upper subplot) and Ricean (lower subplot) propagation conditions are presented when relying on the pragmatic power allocation strategy. For both NCB and CB precoders, each plot shows the theoretical achievable rate per user (lower bound) derived in previous sections (solid lines), their simulated counterparts using (17)-(18) (markers) and the estimated true rates given by

$$\hat{R}_k^{\mathrm{BF}} = \frac{\tau_d}{\tau_c}\mathbb{E}\left\{\log_2\left(1 + \frac{|\mathrm{DS}_k|^2}{|\mathrm{BU}_k|^2 + \sum\limits_{k' \neq k}|\mathrm{UI}_{kk'}|^2 + \sigma_d^2}\right)\right\}. \tag{54}$$

The latter two have been computed using Monte Carlo simulation over 1000 scenarios with 500 fast fading channel realizations/scenario. Several key facts are worth noting. Firstly, and as somewhat expected, a perfect agreement between the analytical and simulated achievable rate is observed for the CB whereas the approximations incurred when deriving theoretical expressions for NCB are found to be very tight (in fact, virtually perfect for the case of Ricean fading). Secondly, and irrespective of the propagation model, the significantly smaller gap between the achievable and the true rates for the case of NCB in comparison to those observed for CB, are already indicative that NCB precoding results in a much more pronounced channel hardening effect. Finally, contrasting the upper and lower plots of Fig. 2a, it can be concluded that LOS propagation is a key factor towards the improvement of the hardening coefficient, thus implying that the achievable rate bounds are indeed more representative of the truly achieved rate in a Ricean environment than in the Rayleigh counterparts. To further confirm the insights drawn from Fig. 2a, the hardening ratio is depicted in Fig. 2b for both precoders under the spatially correlated Rayleigh and Ricean propagation conditions using the analytic expressions proposed in (40) and (42) and contrasting them via Monte Carlo simulations. It can indeed be observed how Ricean propagation and NCB precoding entail a much larger degree of hardening, and in fact, when these two conditions concur, the resulting hardening ratio (well below 0.01) provides an indication that the achievable per-user rate is indeed a tight approximation of the per-user rate achieved in practice. Interestingly, the channel hardening observed under Ricean propagation conditions is almost independent of the network load whereas when Rayleigh fading is assumed, increasing the number of MSs in the network seriously compromises the hardening assumption, most notably for the CB precoder. In fact, in light of these results, the application of the widely used achievable rate bounds appear to be rather inadequate when assessing Rayleigh propagation as it considerably underestimates the true network performance. In contrast, realistic scenarios where LOS condition prevails, specially when using the short-term power constrained precoding scheme, can be accurately assessed by the proposed closed-form bounds. Even though the qualitative result that channel hardening is much consequential in Ricean fading channels is not that surprising, quantifying

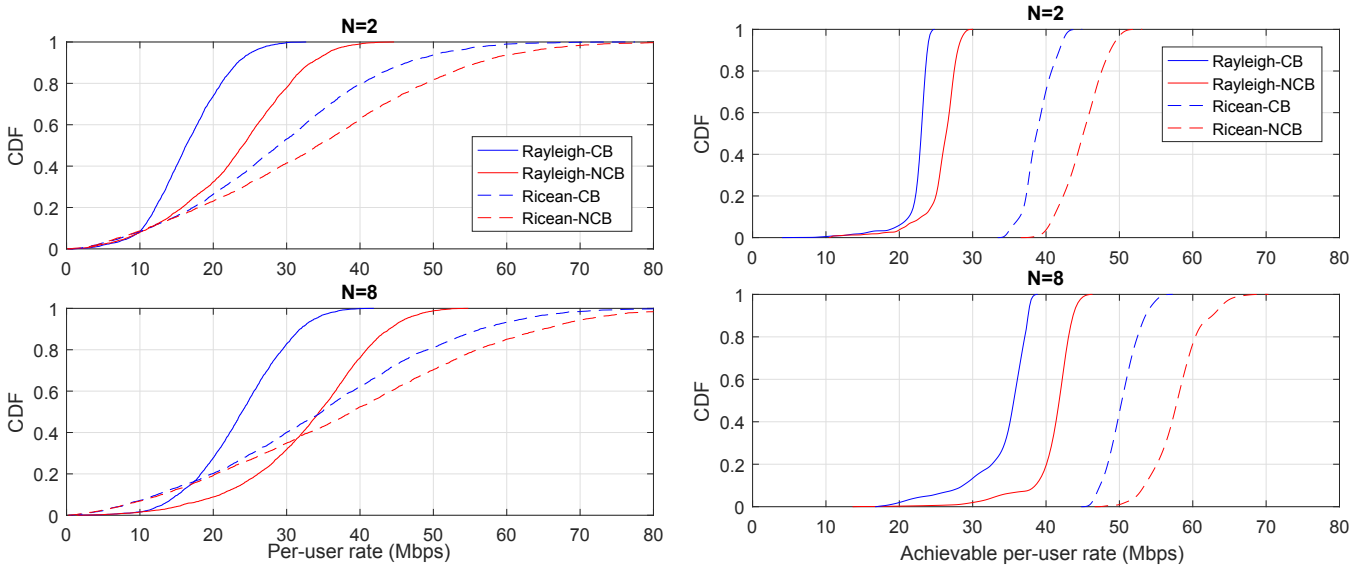

(a) Heuristic power allocation

(b) Max-min power allocation

Fig. 1: CDF of the achievable per-user rate for NCB and CB under Rayleigh and Ricean channels for $K = 25$ MSs and $M = 100$ APs and assuming either pragmatic or max-min power allocation.

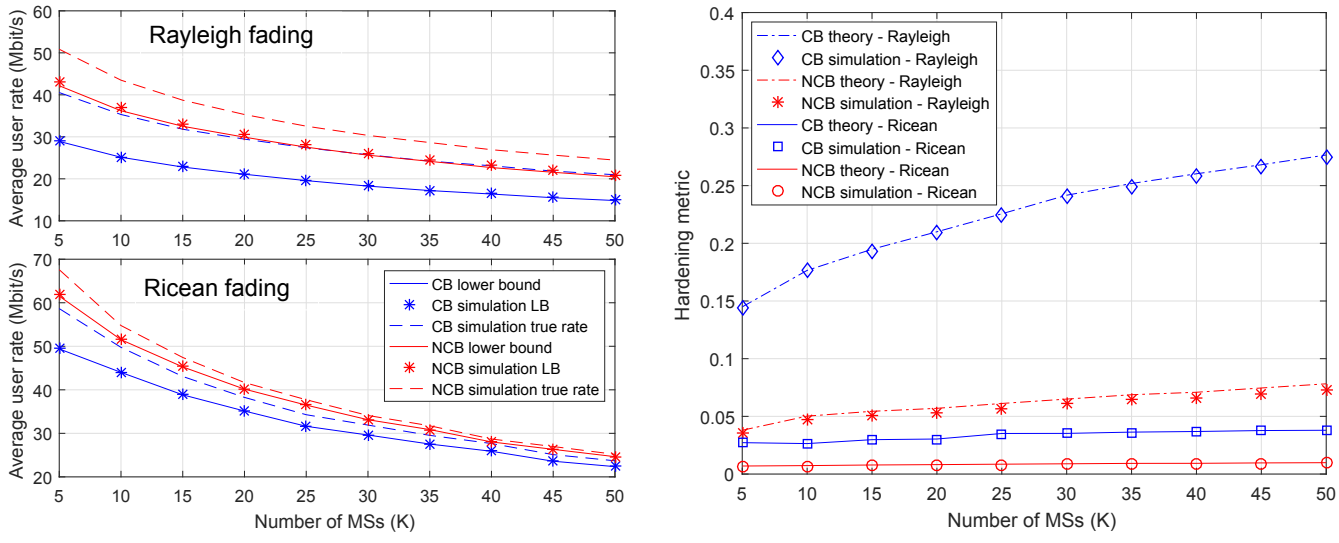

(a) Spectral efficiency metrics

(b) Hardening ratio

Fig. 2: Spectral efficiency metrics and hardening ratio as a function of the number of MSs in a cell-free massive network with $M = 100$ APs all equipped with $N = 4$ antennas.

up to what extent increasing the Rice-K factor improves the hardening ratio in a realistic environment and, even more important, up to what extent improving the hardening ratio also serves to reduce the gap between the closed-form achievable rates and the true rates provided by these systems is of capital importance. Note that, for instance, the max-min power allocation strategies can only be implemented by resorting to closed-form achievable rate expressions and, for obvious reasons, it is highly desirable that these be as close as possible to the true-rates.

Figure 3 shows the favourable propagation ratio defined in (43) for both CB (left) and NCB (right) schemes. In order to highlight the effects pilot contamination might produce on this metric, two different pilot allocation schemes are considered, namely, the aforementioned DCPA strategy, and a naive scheme in which, on the one hand, for those cases in which $K \leq \tau_p$ each MS is allocated an orthogonal pilot sequence and, on the other hand, for those cases in which $K > \tau_p$ there are τ_p MSs that are allocated the τ_p orthogonal pilot sequences, and each of the remaining $K - \tau_p$ MSs is allocated a pilot sequence randomly selected from the pool of available orthogonal ones. Results presented in this figure have been generated for a correlated Ricean channel with ASD $= 10^\circ$ and assuming APs equipped with $N = 4$ antennas and serving $K = 30$ MSs. Since $\tau_p = 20$, there are 10 MSs that do not share their allocated pilot sequence whereas each

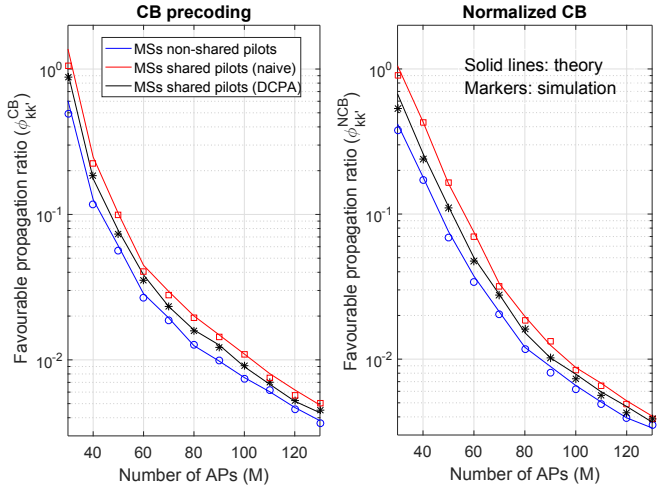

Fig. 3: Favourable propagation ratio as a function of the number of APs, all equipped with $N = 4$ antennas, in a cell-free massive network with $K = 30$ MSs.

of the remaining 20 MSs share their training sequence with at least another MS thus suffering from pilot contamination (i.e., there are 10 MSs with differentiated pilots and 20 MSs with shared pilots). The first important remark that can be drawn from these results is that irrespective of the precoder or pilot allocation strategy under use, increasing the number of APs leads to an improvement of the favourable propagation ratio, which in turn implies that orthogonality among channels experienced by different MSs is effectively ameliorated when increasing the number of APs. As anticipated by the analytical results, MSs with differentiated pilot sequences exhibit a better favourable propagation ratio than those sharing training sequences. This issue, which is tightly related to pilot contamination, can somehow be partially addressed by using a robust form of pilot allocation technique such as the DCPA (black curves) instead of the naive scheme (red curves) that does not take into account the large-scale propagation *fingerprints* of MSs when assigning pilots. As hinted from analytical results derived for the particular case of spatially uncorrelated Rayleigh fading, no significant differences are appreciated between the favourable propagation ratios obtained using CB or NCB strategies, thus confirming that this property is also valid for spatially correlated Ricean fading scenarios and suggesting that the normalization undergone in NCB does not compromise the favourable propagation effect observed as the number of APs increases in a cell-free massive MIMO network.

A recurring dilemma in the cell-free massive MIMO literature is whether it is more advantageous to deploy fewer APs with more antennas or more APs with fewer antennas. Figure 4 shows the spectral efficiency (user achievable rate in solid lines and true rates in dashed lines) for different combinations of N and M always subject to the constraint that $M \times N = 400$ (i.e., 400 transmit antennas in the network) for both NCB and CB precoders. Clearly, when using the NCB strategy (see Fig. 4a), increasing the number of APs at the cost of reducing their complexity (less antennas) is beneficial from the point of view of spectral efficiency. This is indeed indicative of the intrinsic benefit of cell-free systems, namely, bringing the antennas physically closer to the users is always beneficial, a goal that is effectively implemented by distributing the RF front ends as uniformly as possible throughout the coverage area. A potential caveat of the fully distributed configuration ($M = 400$ APs, $N = 1$ antenna/AP) when confronted with the less distributed one ($M = 50$ APs, $N = 8$ antennas/AP), however, is the growing gap between achievable and true rates, a fact already hinted in Fig. 2b. Recall that achievable rates are of paramount importance for governing various optimization procedures, including the power allocation and the pilot assignment processes, hence the importance in having them in the form of tight closed-form expressions. Remarkably, as Fig. 4a reveals, achievable rates for the NCB-case lie within a 5% of the true rate for even the most distributed form. In contrast, the same results are presented in Fig. 4b for the CB-case where the effect of AP distribution is shown to have a devastating effect on the accuracy of the lower bounds based on the achievable rate, as already predicted by results presented in Fig. 2b. Although not shown here, fixing the overall network power and dividing it by the number of APs, a decision that seems to be somehow reasonable when comparing network scenarios with different number of APs, does not alter the results in Figs. 4a and 4b given that acceptable performance levels are always attained in the interference-limited regime.

In order to further explore the advantages of cell-free massive MIMO networks using short-term power constraints, Fig. 5 shows the performance of NCB and CB when varying the number of APs for a fixed number of $K = 25$ MSs in the system. The results help visualizing two facts. Firstly, adding APs to the system is always beneficial irrespective of the particular precoding strategy under use. Secondly, the relative difference (i.e., measured as a percentage of variation) between true and achievable rates shrinks with increasing number of APs, thus confirming that a large number of APs improves channel hardening. As expected, NCB outperforms CB in terms of per-user rate and accuracy of the lower bounds based on the achievable rate analytical expressions. As a concluding remark about hardening that further highlights the advantages of NCBs, we note that results shown in Figs. 4a-5 correspond to the case of Ricean fading, a condition that, as it has been mentioned, is far more favourable in terms of channel hardening ratio than the Rayleigh environment. In particular, the hardening ratio attained by the CB strategy suggests that the corresponding achievable rates will greatly underestimate the true ones up to the point of making it questionable the convenience of using the CB achievable rate expressions for system optimization.

Finally, Fig. 6 explores the effect the ASD around the AoA has on the spectral efficiency performance for the NCB-based scenario (qualitatively similar results are obtained for the CB case) when evaluating different number of serving APs and a fixed number of K=15 MSs. As (53) shows, the ASD $\sigma_{\zeta_{mk}}$ conditions the spatial correlation of the AoA, with increasing angular deviation implying diminishing spa-

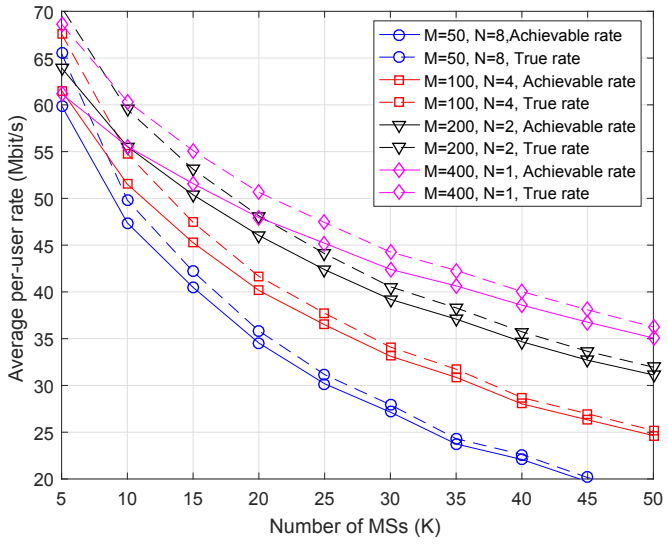

(a) Normalized conjugate beamforming

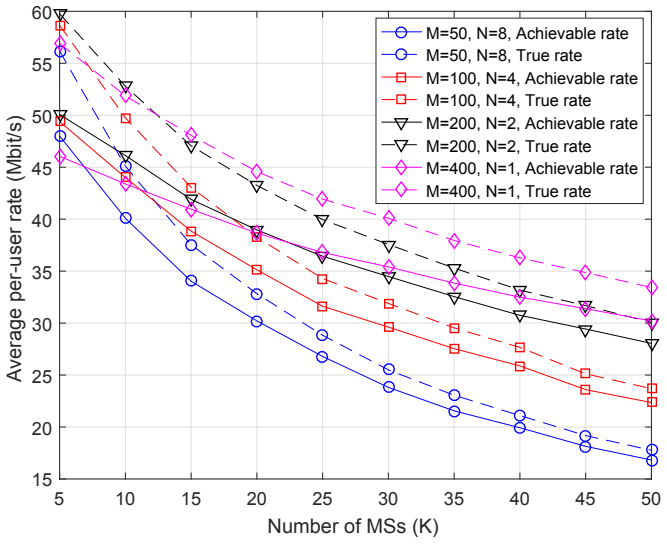

(b) Conjugate beamforming

Fig. 4: Spectral efficiency as a function of the number of MSs in the network for various configurations of M and N subject to $M \times N = 400$.

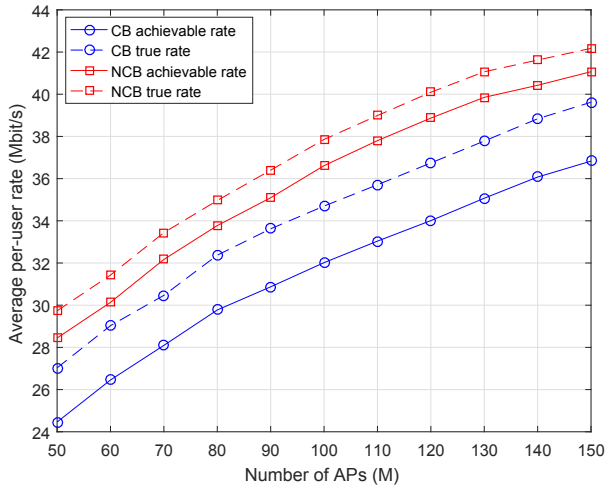

Fig. 5: Spectral efficiency as a function of the number of APs in the network for NCB and CB precoding with Heuristic power allocation and $K = 25$ MSs.

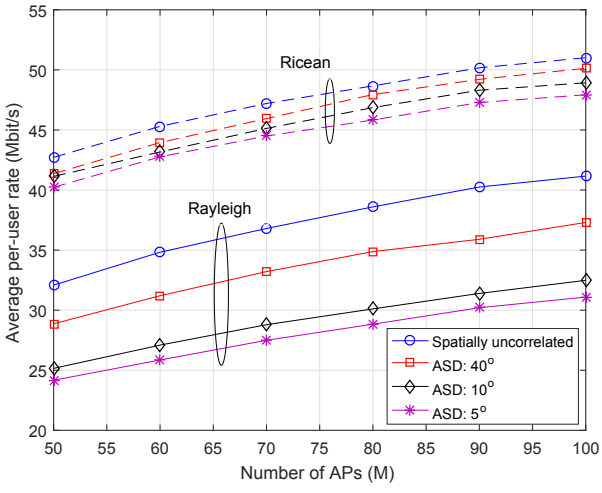

Fig. 6: Spectral efficiency *versus* the number of APs (equipped with $N = 4$ antennas) as a function of the angular spread for NCB precoding with Heuristic power allocation and $K = 15$ MSs.

tial correlation. Results are shown for Rayleigh and Ricean propagation conditions and, for benchmark purposes, results for spatially uncorrelated antenna arrays are also shown. As expected, decreasing spatial correlation leads to a consistent and considerable improvement in performance for the case of the Rayleigh channel. For instance, a cell-free massive MIMO network with $M = 90$ APs each equipped with $N = 4$ antennas can provide an average per-user rate of approximately 30 Mbit/s to only $K = 15$ active MSs under very strong spatially correlated Rayleigh fading (i.e., $\sigma_\zeta = 5^o$). The same spectral efficiency can be provided by a network of $M = 55$ active APs under weak spatially correlated Rayleigh fading (i.e, $\sigma_\zeta = 40^o$). When channel fading conforms to a spatially correlated Ricean model, the same effect is observed although to a milder extent. Note that in this latter case, angular spread plays a less decisive role since the LOS component, which is assumed to be perfectly known at both the transmitter and receiver sides, is unaffected by the spatial correlation matrix.

VI. Conclusion

In this paper, the effects a spatially correlated Ricean fading channel may have on the performance metrics of a cell-free massive MIMO network have been explored. Rigorous exact and approximate closed-form expressions for the downlink achievable rate have been derived assuming the use of both long- and short-term power constraints. These analytical expressions have then been used to evaluate power allocation

strategies based on both pragmatic and optimal max-min per-user rate criteria and have served to gain theoretical insight on the performance advantage provided by the use of short-term power constraints when designing the MIMO precoding strategies.

Large differences observed between the performance metrics obtained under spatially correlated Rayleigh and Ricean fading scenarios have revealed the importance of considering the use of Ricean fading channel models when designing ultradense networks such as those postulated by the cell-free massive MIMO paradigm. Furthermore, the conventional CB scheme, which is based on long-term power constraints, has been shown to be clearly outperformed by the proposed NCB strategy, which uses short-term power constraints. Indeed, the concurrence of spatially correlated Ricean propagation and the use of NCB precoding has been shown to provide a large degree of channel hardening and favourable propagation, thus clearly indicating that closed-form analytical expressions of the achievable rates can be safely assumed to be tight approximations of the rates achieved in practice. The superiority of the NCB precoder has been evidenced under pragmatic power control strategies but it has been even more substantiated when implementing power allocation policies based on the max-min per-user rate criterion. Finally, it has been shown that decreasing spatial correlation leads to a consistent and considerable improvement in performance for the case of the Rayleigh channel model. However, when channel fading conforms to a spatially correlated Ricean model, results revealed that the spatial correlation of the fading seems to have a milder effect on the performance of the system.

APPENDIX A
PROOF OF LEMMA 3

The complex Gaussian random vector $\boldsymbol{x} \sim \mathcal{CN}_N(\boldsymbol{\mu}, \boldsymbol{R})$ can be expressed in terms of a circularly symmetric Gaussian random vector $\boldsymbol{v} \sim \mathcal{CN}_N(\boldsymbol{0}, \boldsymbol{I}_N)$ as $\boldsymbol{x} = \boldsymbol{\mu} + \boldsymbol{R}^{1/2}\boldsymbol{v}$. Thus, the Hermitian quadratic form $\delta = \boldsymbol{x}^H \boldsymbol{H} \boldsymbol{x}$ can be decomposed as

$$\begin{aligned}\delta &= \left(\boldsymbol{\mu} + \boldsymbol{R}^{1/2}\boldsymbol{v}\right)^H \boldsymbol{H} \left(\boldsymbol{\mu} + \boldsymbol{R}^{1/2}\boldsymbol{v}\right) \\ &= \left(\boldsymbol{R}^{-1/2}\boldsymbol{\mu} + \boldsymbol{v}\right)^H \boldsymbol{R}^{H/2}\boldsymbol{H}\boldsymbol{R}^{1/2} \left(\boldsymbol{R}^{-1/2}\boldsymbol{\mu} + \boldsymbol{v}\right).\end{aligned} \tag{55}$$

As the matrix $\boldsymbol{C} = \boldsymbol{R}^{H/2}\boldsymbol{H}\boldsymbol{R}^{1/2}$ is Hermitian, it can be diagonalized as $\boldsymbol{C} = \boldsymbol{U}\boldsymbol{\Lambda}\boldsymbol{U}^H$, where $\boldsymbol{U}$ is unitary and $\boldsymbol{\Lambda} = \mathrm{diag}\left(\left[\lambda_1 \ \ldots \ \lambda_N\right]^T\right)$ is a diagonal matrix containing the eigenvalues of $\boldsymbol{C}$ in its main diagonal. Hence, the Hermitian quadratic form δ can be rewritten as

$$\begin{aligned}\delta &= \left(\boldsymbol{R}^{-1/2}\boldsymbol{\mu} + \boldsymbol{v}\right)^H \boldsymbol{U}\boldsymbol{\Lambda}\boldsymbol{U}^H \left(\boldsymbol{R}^{-1/2}\boldsymbol{\mu} + \boldsymbol{v}\right) \\ &= \left(\overline{\boldsymbol{\mu}} + \boldsymbol{z}\right)^H \boldsymbol{\Lambda} \left(\overline{\boldsymbol{\mu}} + \boldsymbol{z}\right) = \sum_{i=1}^{N} \lambda_i w_i,\end{aligned} \tag{56}$$

where $\overline{\boldsymbol{\mu}} = \boldsymbol{U}^H\boldsymbol{R}^{-1/2}\boldsymbol{\mu} = [\overline{\mu}_1 \ldots \overline{\mu}_N]^T$, $\boldsymbol{z} = \boldsymbol{U}^H\boldsymbol{v} = [z_1 \ \ldots \ z_N]^T$, and $w_i = \left|\overline{\mu}_i + z_i\right|^2$. Since $\boldsymbol{U}$ is unitary, then $\boldsymbol{z} \sim \mathcal{CN}_N(\boldsymbol{0}, \boldsymbol{I}_N)$ and, thus, the Hermitian quadratic form has been expressed as a weighted sum of independent complex chi-square random variables $w_i \sim \mathbb{C}\chi_1^2\left(\left|\overline{\mu}_i\right|^2\right)$.

Although there is no known closed-form expression for the probability density function of a weighted sum of independent complex chi-square random variables, there are many good approximations providing different tradeoffs on the accuracy *versus* computational efficiency/maneagibility plane (see, for instance, [40] and references therein). As we are only interested in obtaining a good approximation to the fractional (1/2)st (non-central) moment of the Hermitian quadratic form δ, the Patnaik's two moment central chi-square approximation [41] will be considered in this paper. Based on Patnaik's approach, δ is approximated by an adjusted random variable $\overline{\delta} = a\xi$, where $\xi \sim \mathbb{C}\chi_\omega^2$, with the parameters a and ω being chosen so that the first two moments of δ and $\overline{\delta}$ coincide. The first two moments of δ can be obtained using Lemma 2 as μ_δ and σ_δ^2, defined in (24) and (25), respectively. Furthermore, as the pdf of $\overline{\delta} = a\xi$ can be expressed as [42]

$$p_{\overline{\delta}}(x) = \frac{1}{a\Gamma(\omega)}\left(\frac{x}{a}\right)^{\omega-1} e^{-x/a}u(x), \tag{57}$$

where $u(x)$ represents the unit step function, the first and second moments of $\overline{\delta}$ can be obtained as

$$\mu_{\overline{\delta}} = \mathbb{E}\{\overline{\delta}\} = \omega a, \tag{58}$$

and

$$\sigma_{\overline{\delta}}^2 = \mathbb{E}\{\left|\overline{\delta} - \mu_{\overline{\delta}}\right|^2\} = \omega a^2, \tag{59}$$

respectively. Now, fitting the first two moments of δ and $\overline{\delta}$ yields

$$a = \frac{\sigma_\delta^2}{\mu_\delta}, \qquad \omega = \frac{\mu_\delta^2}{\sigma_\delta^2}, \tag{60}$$

and the fractional (1/2)st moment of δ can then be approximated as

$$\begin{aligned}\mathbb{E}\left\{\delta^{1/2}\right\} \approx \mathbb{E}\left\{\overline{\delta}^{1/2}\right\} &= \int_{-\infty}^{\infty} x^{1/2} p_{\overline{\delta}}(x)dx \\ &= \sqrt{a}\frac{\Gamma(\omega + 1/2)}{\Gamma(\omega)}.\end{aligned} \tag{61}$$

APPENDIX B
PROOF OF THEOREM 1

Assuming the use of the normalized conjugate beamformer defined in (11), the desired term can be obtained by substituting

$$\begin{aligned}A_{mk}^{\text{NCB}} &= \mathbb{E}\left\{\left(\hat{\boldsymbol{g}}_{mk}^T + \tilde{\boldsymbol{g}}_{mk}^T\right)\frac{\hat{\boldsymbol{g}}_{mk}^*}{\|\hat{\boldsymbol{g}}_{mk}\|}\right\} \\ &= \mathbb{E}\left\{\|\hat{\boldsymbol{g}}_{mk}\|\right\} = \mathbb{E}\left\{\delta_{mk}^{1/2}\right\}\end{aligned} \tag{62}$$

in (14). As $\delta_{mk} = \|\hat{\boldsymbol{g}}_{mk}\|^2$ is a Hermitian quadratic form, Lemma 3 can be applied to accurately approximate this constant as in (29).

The fact that $\boldsymbol{g}_{mk} = \hat{\boldsymbol{g}}_{mk} + \tilde{\boldsymbol{g}}_{mk}$ can be used to expand the interference term due to beamforming gain uncertainty as

$$\begin{aligned}
&\mathbb{E}\left\{\left|\mathrm{BU}_k\right|^2\right\} \\
&= P_d \left[\sum_{m=1}^{M}\sum_{n=1}^{M}\sqrt{\eta_{mk}\eta_{nk}}\,\mathbb{E}\left\{\boldsymbol{g}_{mk}^H\frac{\hat{\boldsymbol{g}}_{mk}}{\|\hat{\boldsymbol{g}}_{mk}\|}\frac{\hat{\boldsymbol{g}}_{nk}^H}{\|\hat{\boldsymbol{g}}_{nk}\|}\boldsymbol{g}_{nk}\right\}\right. \\
&\qquad \left. - \left|\sum_{m=1}^{M}\sqrt{\eta_{mk}}\,\mathbb{E}\left\{\boldsymbol{g}_{mk}^H\frac{\hat{\boldsymbol{g}}_{mk}}{\|\hat{\boldsymbol{g}}_{mk}\|}\right\}\right|^2\right] \\
&= P_d\sum_{m=1}^{M}\eta_{mk}\left(\mathbb{E}\left\{\tilde{\boldsymbol{g}}_{mk}^H\mathbb{E}\left\{\frac{\hat{\boldsymbol{g}}_{mk}\hat{\boldsymbol{g}}_{mk}^H}{\|\hat{\boldsymbol{g}}_{mk}\|^2}\right\}\tilde{\boldsymbol{g}}_{mk}\right\}\right. \\
&\qquad \left. + \mathbb{E}\left\{\delta_{mk}\right\} - \left(\mathbb{E}\left\{\delta_{mk}^{1/2}\right\}\right)^2\right).
\end{aligned} \tag{63}$$

The major difficulty in obtaining a closed-form expression for this term is the calculation of the expectation of the matrix $\hat{\boldsymbol{g}}_{mk}\hat{\boldsymbol{g}}_{mk}^H/\left\|\hat{\boldsymbol{g}}_{mk}\right\|^2$. In order to circumvent this issue, the first order Taylor approximation of the expectation of this quotient will be exploited[3]. That is,

$$\mathbb{E}\left\{\frac{\hat{\boldsymbol{g}}_{mk}\hat{\boldsymbol{g}}_{mk}^H}{\left\|\hat{\boldsymbol{g}}_{mk}\right\|^2}\right\} \approx \frac{\mathbb{E}\left\{\hat{\boldsymbol{g}}_{mk}\hat{\boldsymbol{g}}_{mk}^H\right\}}{\mathbb{E}\left\{\left\|\hat{\boldsymbol{g}}_{mk}\right\|^2\right\}} = \frac{\overline{\boldsymbol{g}}_{mk}\overline{\boldsymbol{g}}_{mk}^H + \boldsymbol{\Phi}_{mk}}{\mathbb{E}\left\{\delta_{mk}\right\}}. \tag{64}$$

Now, using Lemma 2 and the definitions of $\mathbb{E}\left\{\delta_{mk}\right\}$ and $\mathbb{E}\left\{\delta_{mk}^{1/2}\right\}$, the constant B_{mk}^{NCB} in (30) can be directly obtained.

The interuser interference terms can be obtained as

$$\begin{aligned}
&\mathbb{E}\left\{\left|\mathrm{UI}_{kk'}\right|^2\right\} \\
&= P_d\sum_{m=1}^{M}\sum_{n=1}^{M}\sqrt{\eta_{mk'}\eta_{nk'}}\,\mathbb{E}\left\{\boldsymbol{g}_{mk}^H\frac{\hat{\boldsymbol{g}}_{mk'}}{\|\hat{\boldsymbol{g}}_{mk'}\|}\frac{\hat{\boldsymbol{g}}_{nk'}^H}{\|\hat{\boldsymbol{g}}_{nk'}\|}\boldsymbol{g}_{nk}\right\} \\
&= P_d\left[\sum_{m=1}^{M}\eta_{mk'}\,\mathbb{E}\left\{\frac{\boldsymbol{g}_{mk}^H\hat{\boldsymbol{g}}_{mk'}\hat{\boldsymbol{g}}_{mk'}^H\boldsymbol{g}_{mk}}{\|\hat{\boldsymbol{g}}_{mk'}\|^2}\right\}\right. \\
&\quad \left. + \sum_{m=1}^{M}\sum_{\substack{n=1\\n\neq m}}^{M}\sqrt{\eta_{mk'}\eta_{nk'}}\,\mathbb{E}\left\{\frac{\boldsymbol{g}_{mk}^H\hat{\boldsymbol{g}}_{mk'}}{\|\hat{\boldsymbol{g}}_{mk'}\|}\right\}\mathbb{E}\left\{\frac{\hat{\boldsymbol{g}}_{nk'}^H\boldsymbol{g}_{nk}}{\|\hat{\boldsymbol{g}}_{nk'}\|}\right\}\right]
\end{aligned} \tag{65}$$

and, again, the expectations of quotients can be approximated by resorting to the use of first order Taylor approximations as

$$\begin{aligned}
&\mathbb{E}\left\{\left|\mathrm{UI}_{kk'}\right|^2\right\} \\
&\approx P_d\left[\sum_{m=1}^{M}\eta_{mk'}\frac{\mathbb{E}\left\{\boldsymbol{g}_{mk}^H\hat{\boldsymbol{g}}_{mk'}\hat{\boldsymbol{g}}_{mk'}^H\boldsymbol{g}_{mk}\right\}}{\mathbb{E}\left\{\left\|\hat{\boldsymbol{g}}_{mk'}\right\|^2\right\}}\right. \\
&\quad \left. + \sum_{m=1}^{M}\sum_{\substack{n=1\\n\neq m}}^{M}\sqrt{\eta_{mk'}\eta_{nk'}}\frac{\mathbb{E}\left\{\boldsymbol{g}_{mk}^H\hat{\boldsymbol{g}}_{mk'}\right\}}{\mathbb{E}\left\{\|\hat{\boldsymbol{g}}_{mk'}\|\right\}}\frac{\mathbb{E}\left\{\hat{\boldsymbol{g}}_{nk'}^H\boldsymbol{g}_{nk}\right\}}{\mathbb{E}\left\{\|\hat{\boldsymbol{g}}_{nk'}\|\right\}}\right].
\end{aligned} \tag{66}$$

Using (1) and (5), applying Lemma 2, and exploiting the mathematical expressions of $\mathbb{E}\{\delta_{mk'}\}$ and $\mathbb{E}\{\delta_{mk'}^{1/2}\}$, these terms can be expressed as

$$\begin{aligned}
&\mathbb{E}\left\{\left|\mathrm{UI}_{kk'}\right|^2\right\} \\
&= P_d\sum_{m=1}^{M}\frac{\eta_{mk'}}{\mu_{\delta_{mk'}}}\left[\left|\overline{\boldsymbol{g}}_{mk}^H\overline{\boldsymbol{g}}_{mk'}\right|^2 + \overline{\boldsymbol{g}}_{mk}^H\boldsymbol{\Phi}_{mk'}\overline{\boldsymbol{g}}_{mk}\right. \\
&\quad + \left|\overline{\boldsymbol{g}}_{mk'}^H\boldsymbol{R}_{mk}^{1/2}\overline{\boldsymbol{g}}_{mk}\right|^2 + \overline{\boldsymbol{g}}_{mk'}^H\boldsymbol{R}_{mk}\overline{\boldsymbol{g}}_{mk'} \\
&\quad + \left|\mathrm{tr}\left(\boldsymbol{R}_{mk}\boldsymbol{\Phi}_{mk'}\boldsymbol{R}_{mk'}^{-1}\right)\right|^2\left|\boldsymbol{\varphi}_k^H\boldsymbol{\varphi}_{k'}\right|^2 + \mathrm{tr}\left(\boldsymbol{R}_{mk}\boldsymbol{\Phi}_{mk'}\right) \\
&\quad \left. + 2\Re\left\{\overline{\boldsymbol{g}}_{mk'}^H\overline{\boldsymbol{g}}_{mk}\,\mathrm{tr}\left(\boldsymbol{R}_{mk}\boldsymbol{\Phi}_{mk'}\boldsymbol{R}_{mk'}^{-1}\right)\right\}\boldsymbol{\varphi}_k^H\boldsymbol{\varphi}_{k'}\right] \\
&\quad + P_d\sum_{m=1}^{M}\sum_{\substack{n=1\\n\neq m}}^{M}\frac{\sqrt{\eta_{mk'}\eta_{nk'}}}{A_{mk'}^{\mathrm{NCB}}A_{nk'}^{\mathrm{NCB}}} \\
&\quad \times\left(\overline{\boldsymbol{g}}_{mk}^H\overline{\boldsymbol{g}}_{mk'} + \mathrm{tr}\left(\boldsymbol{R}_{mk}\boldsymbol{\Phi}_{mk'}\boldsymbol{R}_{mk'}^{-1}\right)\boldsymbol{\varphi}_k^H\boldsymbol{\varphi}_{k'}\right) \\
&\quad \times\left(\overline{\boldsymbol{g}}_{nk'}^H\overline{\boldsymbol{g}}_{nk} + \mathrm{tr}\left(\boldsymbol{R}_{nk'}^{-1}\boldsymbol{\Phi}_{nk'}\boldsymbol{R}_{nk}\right)\boldsymbol{\varphi}_{k'}^H\boldsymbol{\varphi}_k\right).
\end{aligned} \tag{67}$$

A straightforward rearrangement of terms leads to the interuser interference terms in (28), where the constants $C_{mkk'}^{\mathrm{NCB}}$ and $D_{mkk'}^{\mathrm{NCB}}$ in (31) and (32) can be readily identified.

Acknowledgements: Work supported in part by the Agencia Estatal de Investigación (AEI) of Spain under Grants TEC2017-90093-C3-2-R and TEC2017-90093-C3-3-R, and in part by the European Regional Development Fund (ERDF) funds of the European Union (EU) (AEI/FEDER, UE).

[3]Note that using higher order Taylor approximations has its own issues when trying to obtain closed-form expressions. Furthermore, as shown in the numerical results section, analytical results obtained using the first order Taylor approximation are so accurate, when compared to Monte Carlo simulation results, that make it superfluous the analytical burden associated to higher order approximations.

REFERENCES

[1] E. G. Larsson, O. Edfors, F. Tufvesson, and T. L. Marzetta, "Massive MIMO for next generation wireless systems," *IEEE Communications Magazine*, vol. 52, no. 2, pp. 186–195, 2014.

[2] T. Marzetta, E. Larsson, H. Yang, and H. Ngo, *Fundamentals of Massive MIMO*, ser. Fundamentals of Massive MIMO. Cambridge University Press, 2016.

[3] L. Lu, G. Y. Li, A. L. Swindlehurst, A. Ashikhmin, and R. Zhang, "An overview of massive MIMO: Benefits and challenges," *IEEE Journal of Selected Topics in Signal Processing*, vol. 8, no. 5, pp. 742–758, 2014.

[4] H. Q. Ngo, A. Ashikhmin, H. Yang, E. G. Larsson, and T. L. Marzetta, "Cell-free massive MIMO versus small cells," *IEEE Transactions on Wireless Communications*, vol. 16, no. 3, pp. 1834–1850, 2017.

[5] W. Choi and J. G. Andrews, "Downlink performance and capacity of distributed antenna systems in a multicell environment," *IEEE Transactions on Wireless Communications*, vol. 6, no. 1, pp. 69–73, Jan 2007.

[6] M. K. Karakayali, G. J. Foschini, and R. A. Valenzuela, "Network coordination for spectrally efficient communications in cellular systems," *IEEE Wireless Communications*, vol. 13, no. 4, pp. 56–61, Aug 2006.

[7] D. Gesbert, S. Hanly, H. Huang, S. S. Shitz, O. Simeone, and W. Yu, "Multi-cell MIMO cooperative networks: A new look at interference," *IEEE Journal on Selected Areas in Communications*, vol. 28, no. 9, pp. 1380–1408, December 2010.

[8] R. Irmer *et al.*, "Coordinated multipoint: Concepts, performance, and field trial results," *IEEE Communications Magazine*, vol. 49, no. 2, pp. 102–111, February 2011.

[9] A. Checko, H. L. Christiansen, Y. Yan, L. Scolari, G. Kardaras, M. S. Berger, and L. Dittmann, "Cloud RAN for mobile networks - A technology overview," *IEEE Communications Surveys*, vol. 17, no. 1, pp. 405–426, Firstquarter 2015.

[10] H. Q. Ngo, A. Ashikhmin, H. Yang, E. G. Larsson, and T. L. Marzetta, "Cell-free massive MIMO: Uniformly great service for everyone," in *IEEE SPAWC*.

[11] F. Riera-Palou, G. Femenias, A. G. Armada, and A. Pérez-Neira, "Clustered cell-free massive MIMO," in *2018 IEEE Globecom Workshops (GC Wkshps)*, Dec 2018, pp. 1–6.

[12] E. Nayebi, A. Ashikhmin, T. L. Marzetta, H. Yang, and B. D. Rao, "Precoding and power optimization in cell-free massive MIMO systems," *IEEE Transactions on Wireless Communications*, vol. 16, no. 7, pp. 4445–4459, 2017.

[13] S. Buzzi and C. D Andrea, "Cell-free massive MIMO: User-centric approach," *IEEE Wireless Commun. Lett.*, vol. 6, no. 6, pp. 706–709, 2017.

[14] J. Zhang, Y. Wei, E. Björnson, Y. Han, and S. Jin, "Performance analysis and power control of cell-free massive MIMO systems with hardware impairments," *IEEE Access*, vol. 6, pp. 55 302–55 314, Sept 2018.

[15] M. Bashar, K. Cumanan, A. G. Burr, M. Debbah, and H. Q. Ngo, "On the uplink max-min SINR of cell-free massive MIMO systems," *IEEE Transactions on Wireless Communications*, vol. 18, no. 4, pp. 2021–2036, April 2019.

[16] O. Özdogan, E. Björnson, and J. Zhang, "Performance of cell-free massive MIMO with Rician fading and phase shifts," *IEEE Transactions on Wireless Communications*, vol. 18, no. 11, pp. 5299–5315, Nov 2019.

[17] H. Q. Ngo, H. Tataria, M. Matthaiou, S. Jin, and E. G. Larsson, "On the performance of cell-free massive MIMO in Ricean fading," in *52nd Asilomar Conference on Signals, Systems, and Computers*, Oct 2018, pp. 980–984.

[18] E. Björnson and L. Sanguinetti, "Making cell-free massive MIMO competitive with MMSE processing and centralized implementation," *IEEE Transactions on Wireless Communications*, vol. 19, no. 1, pp. 77–90, Jan 2020.

[19] W. Fan, J. Zhang, E. Bjornson, S. Chen, and Z. Zhong, "Performance analysis of cell-free massive MIMO over spatially correlated fading channels," in *IEEE International Conference on Communications (ICC)*, 2019, pp. 1–6.

[20] J. Qiu, K. Xu, X. Xia, Z. Shen, and W. Xie, "Downlink power optimization for cell-free massive MIMO over spatially correlated Rayleigh fading channels," *IEEE Access*, vol. 8, pp. 56 214–56 227, March 2020.

[21] M. Zhou, Y. Zhang, X. Qiao, and L. Yang, "Spatially correlated Rayleigh fading for cell-free massive MIMO systems," *IEEE Access*, vol. 8, pp. 42 154–42 168, 2020.

[22] M. Khoshnevisan and J. N. Laneman, "Power allocation in multi-antenna wireless systems subject to simultaneous power constraints," *IEEE Transactions on Communications*, vol. 60, no. 12, pp. 3855–3864, December 2012.

[23] G. Interdonato, H. Q. Ngo, E. G. Larsson, and P. Frenger, "On the performance of cell-free massive MIMO with short-term power constraints," in *IEEE 21st International Workshop on Computer Aided Modelling and Design of Communication Links and Networks (CAMAD)*, 2016,.

[24] Y. Zhang, H. Cao, Y. Guo, and L. Yang, "SCA power optimization in cell-free massive MIMO with short-term power constraints," in *2018 10th International Conference on Wireless Communications and Signal Processing (WCSP)*, Oct 2018, pp. 1–6.

[25] Y. Zhang, H. Cao, C. Qi, P. Zhong, and L. Yang, "Power optimization in cell-free massive MIMO with short-term power constraints," in *2018 IEEE 4th International Conference on Computer and Communications (ICCC)*, Dec 2018, pp. 370–376.

[26] G. Femenias and F. Riera-Palou, "Cell-free millimeter-wave massive MIMO systems with limited fronthaul capacity," *IEEE Access*, vol. 7, pp. 44 596–44 612, 2019.

[27] O. Özdogan, E. Björnson, and E. G. Larsson, "Massive MIMO with spatially correlated Rician fading channels," *IEEE Transactions on Communications*, vol. 67, no. 5, pp. 3234–3250, May 2019.

[28] A. Álvarez-Polegre, F. Riera-Palou, G. Femenias, and A. García-Armada, "Channel hardening in cell-free and user-centric massive MIMO networks with spatially correlated Ricean fading," *IEEE Access*, vol. 8, pp. 139 827–139 845, 2020.

[29] G. Interdonato, M. Karlsson, E. Björnson, and E. G. Larsson, "Local partial zero-forcing precoding for cell-free massive MIMO," *IEEE Transactions on Wireless Communications*, vol. 19, no. 7, pp. 4758–4774, 2020.

[30] E. Björnson, J. Hoydis, and L. Sanguinetti, "Massive MIMO networks: Spectral, energy, and hardware efficiency," *Foundations and Trends®in Signal Processing*, vol. 11, no. 3-4, pp. 154–655, 2017.

[31] O. Elijah, C. Y. Leow, T. A. Rahman, S. Nunoo, and S. Z. Iliya, "A comprehensive survey of pilot contamination in massive MIMO-5G system," *IEEE Comm. Surv. & Tutor.*, vol. 18, no. 2, pp. 905–923, 2016.

[32] S. Haghighatshoar and G. Caire, "Massive MIMO pilot decontamination and channel interpolation via wideband sparse channel estimation," *IEEE Transactions on Wireless Communications*, vol. 16, no. 12, pp. 8316–8332, Dec 2017.

[33] D. Neumann, M. Joham, and W. Utschick, "Covariance matrix estimation in massive MIMO," *IEEE Signal Processing Letters*, vol. 25, no. 6, pp. 863–867, 2018.

[34] K. Upadhya and S. A. Vorobyov, "Covariance matrix estimation for massive MIMO," *IEEE Signal Processing Letters*, vol. 25, no. 4, pp. 546–550, 2018.

[35] S. M. Kay, *Fundamentals of statistical signal processing*, ser. Prentice Hall signal processing series. Upper Saddle River, NJ: Prentice Hall PTR, 1993. [Online]. Available: http://cds.cern.ch/record/2012069

[36] S. Park, E. Serpedin, and K. Qaraqe, "Gaussian assumption: The least favorable but the most useful [lecture notes]," *IEEE Signal Processing Magazine*, vol. 30, no. 3, pp. 183–186, 2013.

[37] Z. Chen and E. Björnson, "Channel hardening and favorable propagation in cell-free massive MIMO with stochastic geometry," *IEEE Transactions on Communications*, vol. 66, no. 11, pp. 5205–5219, Nov 2018.

[38] 3GPP, "Study on 3D channel model for LTE (Release 12)," 3GPP TR 36.873 (version 12.7.0), December 2017.

[39] L. Sanguinetti, E. Björnson, and J. Hoydis, "Toward massive MIMO 2.0: Understanding spatial correlation, interference suppression, and pilot contamination," *IEEE Transactions on Communications*, vol. 68, no. 1, pp. 232–257, 2020.

[40] D. A. Bodenham and N. M. Adams, "A comparison of efficient approximations for a weighted sum of chi-squared random variables," *Statistics and Computing*, vol. 26, no. 4, pp. 917–928, 2016.

[41] P. B. Patnaik, "The non-central χ^2- and F-distribution and their applications," *Biometrika*, vol. 36, no. 1/2, pp. 202–232, 1949.

[42] O. Besson and Y. I. Abramovich, "Regularized covariance matrix estimation in complex elliptically symmetric distributions using the expected likelihood approach–Part 2: The under-sampled case," *IEEE Transactions on Signal Processing*, vol. 61, no. 23, pp. 5819–5829, 2013.